UCLouvain

epl

École polytechnique de Louvain

Creation of a controller to simulate biped locomotion with ELSA Prosthesis Digital Twin

Author: **Eliot Paulus**
Supervisors: **Renaud Ronsse, François Herremans**
Reader: **Fisette Paul**
Academic year 2022–2023
Master [120] in Biomedical Engineering

Abstract

The escalating prevalence of amputations, driven by factors such as diabetes-related complications and traumatic incidents necessitates urgent innovative solutions. The rise in global diabetes cases, projected to reach 570.9 million by 2025, contributes to a concerning increase in lower-extremity amputations. The 2016 GBD, Injuries and Risk Factors Study reported 131 million individuals with diabetes-related lower-extremity issues, including 6.8 million amputations and 0.4 million requiring prosthetic interventions.

Prosthetic technology has evolved significantly, transitioning from rudimentary designs to advanced bionic creations. In the last decade, below-knee prostheses have shifted from static structures to dynamic systems mirroring human ankle-foot movement. Two distinct visions have emerged: the first one articulated energy storing and returning (ESR) feet. And bionic feet using hydraulic or electric actuation for natural motion.

The concept of the digital twin, a computational replica of a physical device, holds promise in prosthetic technology advancement. The Efficient Lockable Spring Ankle (ELSA) prosthesis, developed at UCLouvain, embodies this innovation. To replicate natural gait, the SIMBICON controller, rooted in biomechanics and dynamic optimization, is employed and adapted to ELSA's context for accurate simulated gait.

This thesis delves into creating an environment to emulate human gait, detailing research methodology, technical implementations and findings. By developing a digitized environment to simulate human gait, this study contributes to ELSA's advancement. The digital twin concept bridges theoretical innovation and real-world implementation, revolutionizing prosthetic device development and optimization. As medical technology advances, digital twins promise innovative solutions, redefining design, testing and refinement approaches.

Acknowledgments

I would like to express my sincere gratitude to my supervisor, Mr. Renaud Ronsse, for his guidance, and support throughout the entire duration of this research journey. Your expertise and encouragement have been instrumental in shaping the direction and quality of this work.

In addition, I extend my heartfelt thanks to Olivier Lanstoght and François Heremans, whose valuable insights and contributions have greatly enriched the content of this thesis. Your willingness to share your knowledge and provided assistance has been truly invaluable.

I extend my deepest appreciation to my family and close circle of friends for their unwavering support and encouragement. Your belief in my abilities, and your patience of listening to me during those long hours, have provided me with the strength to navigate the challenges of this endeavor.

To everyone who has been a part of this journey, whether directly or indirectly, your presence and contributions were for me of the utmost importance. Thank you from the bottom of my heart.

Contents

List of Figures

List of Tables

Introduction

The escalating prevalence of amputations, increased by factors such as diabetes-related complications and traumatic incidents, underscores the urgent need for innovative solutions. Particularly, the surge in diabetes cases, which forecasts a rise in global diabetes prevalence from 476.0 million to an estimated 570.9 million by 2025 [1], has fueled an alarming increase in lower-extremity amputations.

These alarming factors become even more apparent when examining data from the GBD, Injuries, and Risk Factors Study of 2016. This study reported approximately 131 million individuals, representing nearly 1.8% of the global population, grappling with diabetes-related lower-extremity complications. Among these cases, around 6.8 million amputations were performed, with an additional 0.4 million amputations requiring prosthetic interventions [2].

In response to these challenges, the field of prosthetic technology has undergone transformative growth. The evolution spans from rudimentary, supportive designs to intricate bionic creations. Focusing on below-knee prostheses from the past decade, there has been a notable shift from static, rigid structures to dynamic systems that can replicate human ankle-foot movement. This journey culminates with two different visions of the future of prosthesis. On one hand, there are the articulated energy storing and returning (ESR) feet which engage or disengage a locking mechanism which store energy by loading a spring with the body weight. Despite the precision of their electromechanical systems, they do not use external mechanical power to provide active stability or sagging characteristics to the user. On the other hand, the bionic feet technologies that are defined as a mechanical device with one ore more active ingredients used to stabilize the foot or provide active sagging characteristics. These types of prosthesis use hydraulic or electric actuation to provide natural ankle kinematics and intelligent terrain adaptability but they are not energy-sufficient on the contrary of ESR which tends to be [3].

In this pursuit of enhanced prosthetic technology, the concept of the digital twin appears to hold great promise. A digital twin is a computational replica of a physical device or system. Its potential lies in its ability to revolutionize the design and testing process. By creating a virtual counterpart of a physical prosthesis, researchers can simulate and analyze its behavior under various conditions, leading to refined designs and optimized performance which offers new capabilities.

This innovative approach finds its embodiment in the Efficient Lockable Spring Ankle (ELSA) prosthesis developed by researchers at UCLouvain. The ELSA prosthesis seeks

to address the multiple challenges faced by amputees, ranging from energy efficiency to user comfort and the accurate replication of natural gait patterns while managing an affordable price. At the heart of this research lies the aspiration to develop a digitized environment capable of emulating the intricate dynamics of human locomotion.

To replicate the human locomotion, the choice of a suitable controller is crucial. The SIMBICON controller emerges as a foundational framework for this master thesis. Founded on the principles of biomechanics and dynamic optimization, the SIMBICON controller provides a solid foundation for emulating natural gait patterns. Building upon this established base, this thesis strives to refine and adapt the SIMBICON controller to suit the context of the ELSA prosthesis, aiming to create a simulated human gait that is both accurate and reproducible.

The subsequent chapters of this thesis dive deeper into the intricate details of the elaboration of an environment capable of emulating the human gait. Through a comprehensive exploration of the research methodology, technical implementations and findings, this study aspires to contribute to the advancement of ELSA's prosthesis and prosthetic technology. The goal is to empower individuals who rely on these innovative solutions, fostering enhanced mobility and improving quality of life.

Ultimately, the digital twin concept stands as a bridge between theoretical innovation and real-world implementation, offering the potential to revolutionize the development and optimization of prosthetic devices. As the field of medical technology marches forward, digital twins hold the promise of fundamentally altering the way we approach design, testing and refinement, ultimately leading to more effective solutions for those in need.

Chapter 1

Context

1.1 Digital twins

In recent years, the concept of digital twins (DTs) has gained the attention of various industries, revolutionizing the way products are designed, manufactured, and maintained. As we wan see on Fig. 1.1, over the last decade, the number of articles published per year containing the word "digital twin" has expanded, demonstrating the interest shown by industry and scientists in this technology. A DT is a virtual representation of a physical asset, system, or process that is continuously updated in real-time, mimicking its real-world counterpart's behavior and performance. This technology leverages advancements in simulation, data analytics, and connectivity, enabling industries to achieve unprecedented levels of efficiency, reliability, and innovation[4].

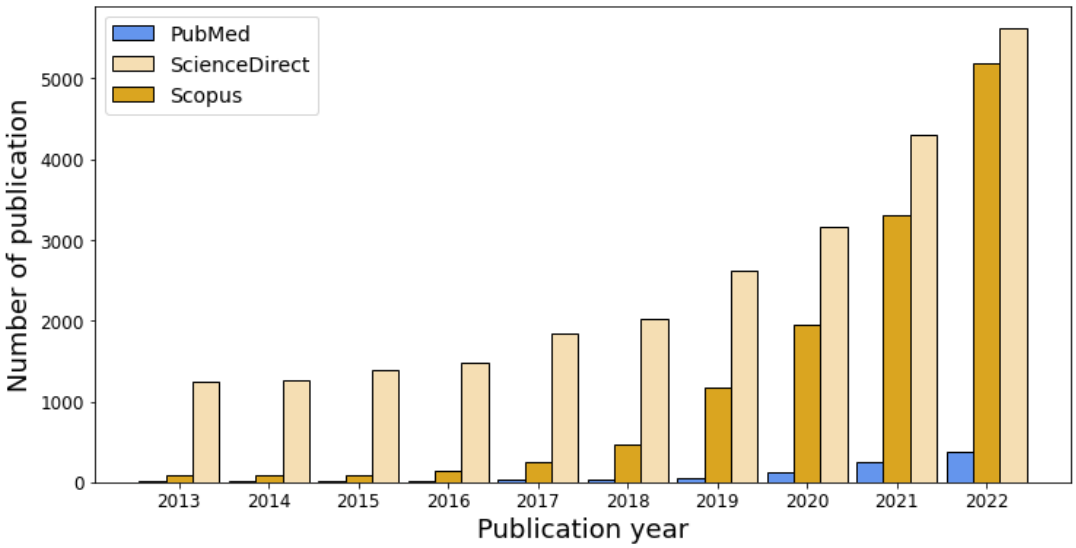

Figure 1.1: Number of Digital Twin-related publications by year frome 2013 to 2022 on Scopus, ScienceDirect & PubMed

1.1.1 Interest of Digital Twins

Manufacturing and product design

The manufacturing sector has embraced DTs as a powerful tool for optimizing product design and production processes. By creating a virtual replica of a product, manufacturers can simulate different design iterations and assess their performance under varying conditions. This able engineers to identify potential flaws, streamline the design process, and ensure that products meet performance requirements before physical prototypes are even built. Moreover, DTs allow for predictive maintenance, as they can forecast component failures based on real-time sensor data, reducing downtime maintenance and minimizing costs of a product cycle of life [5].

Infrastructure and energy

In the infrastructure and energy sector, DTs are crucial in monitoring and managing complex systems. For instance, in the field of renewable energy, wind turbines and solar panels are equipped with sensors that transmit real-time data to their DTs. This data can be used to optimize energy production, detect anomalies, and prevent costly breakdowns [6]. Similarly, DTs are studied in the supervision of smart cities, where they could assist in traffic management, waste disposal and in optimizing energy consumption [7].

Digital Twins in the medical field

The medical field has also embraced the concept of DTs, leveraging their capabilities to enhance patient care, treatment strategies and medical research. The application of DTs in healthcare introduces a new era that enable a more personalized and precise approach to diagnosis, treatment and patient management. The DTs are already influencing the medical domain, and here are a couple of field illustrating these effects:

- **Personalized treatment:** Patient-specific DTs enable tailored treatment strategies, predicting treatment effects on unique patient conditions [8].
- **Surgical planning and training:** The advance in DTs and haptic devices technologies allows surgeons to carefully plan and train their operations on patient specific digital models before the operation. Moreover, the medical students can also benefit from an immersive training [9].

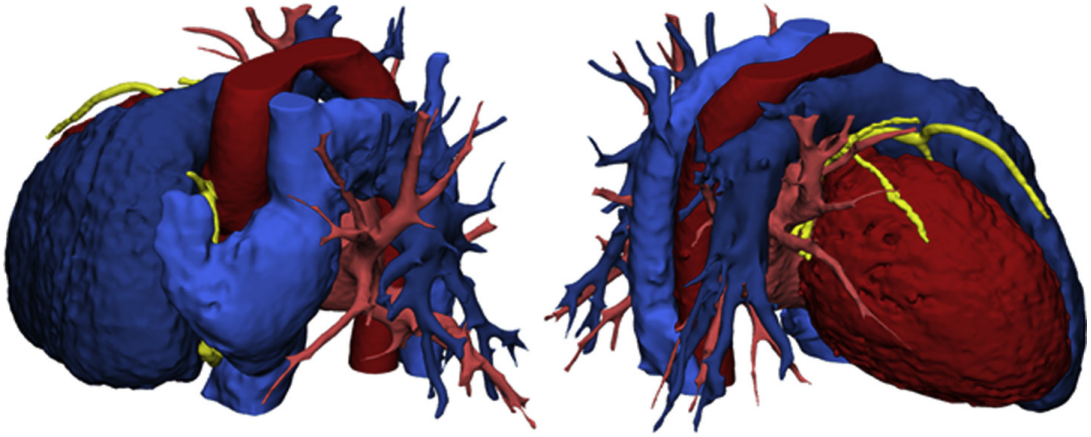

Figure 1.2: A 3-D reconstruction of a patient cardiac blood volumes. Previous underlying dextrocardia and a history of surgical repairs, made much of the patients anatomy abnormal [10].

In conclusion, digital twins transcend industries, significantly impacting healthcare by enabling personalized treatment, improving surgical training and advancing medical research. Pursuing these goals, this master thesis attempts to create a model of the human walk to test the ELSA digital twin in a digitized environment.

1.1.2 Classification of Digital Twins

Digital twins can be classified into different types based on various criteria, including their creation time, level of integration, applications, hierarchy, and maturity level. This classification offers insights into the diverse ways digital twins are employed in different contexts [11].

DT Creation time

Grieves and Vickers [12] outline two fundamental types of digital twins based on their creation time within a product's life cycle: Digital Twin Prototype (DTP) and Digital Twin Instance (DTI).

- **Digital Twin Prototype (DTP):** DTP is established during the design phase and encompasses the data essential for creating or manufacturing a physical counterpart. This type enables testing, including potentially destructive scenarios before the physical twin's production. DTP ensures smoother validation and identification of challenges, resulting in higher-quality physical replicas.
- **Digital Twin Instance (DTI):** DTI is linked to the physical counterpart throughout its life cycle, which is established during the production phase. It enables real-time monitoring and behavior prediction of the physical system. Changes in either the physical or digital twin are mirrored in one another due to bidirectional synchronization.

Level of Integration

Kritzinger et al. [13] classifies digital twins based on their level of integration:

- **Digital model:** In this type, data exchange between the physical and digital versions is manual. Changes in the physical object don't directly reflect in its digital counterpart and vice versa.
- **Digital shadow:** Data from the physical object flow automatically to the digital twin but the reverse process remains manual. Changes in the physical object are visible in its digital representation.
- **Digital twin:** This type features automatic bidirectional data flow between the physical and digital versions. Changes in either object directly impact the other.

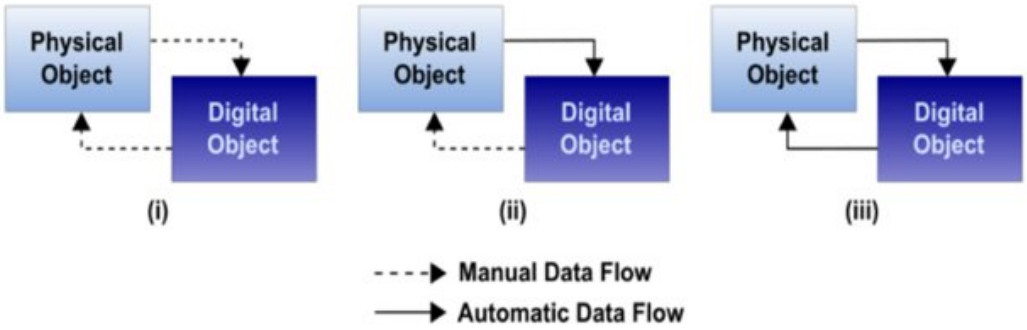

Figure 1.3: Types of DT based on level of integration (from [11]). (i)Digital Model;(ii)Digital shadow/Static DIgital model;(iii)Digital Twin/Dynamic Digital Model.

Application

Digital twins can be classified based on their applications, broadly categorized as **Predictive DT** and **Interrogative DT** [12]. Moreover, they can be divided based on whether their focus of application is on Product, Production, or Performance:

- **Product DT:** Used for prototyping and analysing products under different conditions to ensure they behave as intended.
- **Production DT:** Validates processes through simulation and analysis, helping the development of efficient production methods.
- **Performance DT:** Involves decision-making processes, capturing and analyzing data from smart products and plants to optimize operations.

Hierarchy

Digital twins can be organized hierarchically, encompassing Unit Level, System Level, and System of Systems Level:

- **Unit level:** Represents individual manufacturing components like equipment, materials and environmental factors.
- **System level:** Combines several unit-level digital twins within a production system, enabling better resource allocation and data flow.
- **System of systems level:** Connects system-level digital twins, facilitating collaboration across enterprises and departments.

Sophistication

Digital twins sophistication level increases with accumulated operational data and advanced virtual representations. The maturity level of digital twins can be classified as [14]:

- **Pre-Digital Twin:** Created before the physical asset, assisting decision-making for prototype designs.
- **Digital Twin:** Incorporates data from the physical asset for high-level decision-making, maintenance scheduling and bidirectional data transfer.
- **Adaptive Digital Twin:** Features an adaptive user interface enabling real-time planning and decision-making through supervised machine learning.
- **Intelligent Digital Twin:** Possesses unsupervised machine-learning capability premitting precise and efficient analysis through recognition of operational patterns and reinforced learning.

In conclusion, the classification of digital twins reflects their diversity in creation, integration, application focus, hierarchy and sophistication level. These classifications offer insights into the wide-ranging potential of digital twin technology across industries.

1.2 Simulating the humain gait

Human gait simulation is a complex challenge in biomechanics due to the involved combination of nonlinear human motion equations, muscle dynamics and foot-ground contact. The pursuit of accurate and computationally efficient predictive human gait simulation has driven extensive research in various applications such as surgical intervention planning [15] prosthesis and orthosis design[16]. This section is divided in two main parts, the first one provides a comprehensive overview of the simulation methods. The second one focuses on the different modeling solutions for the human gait.

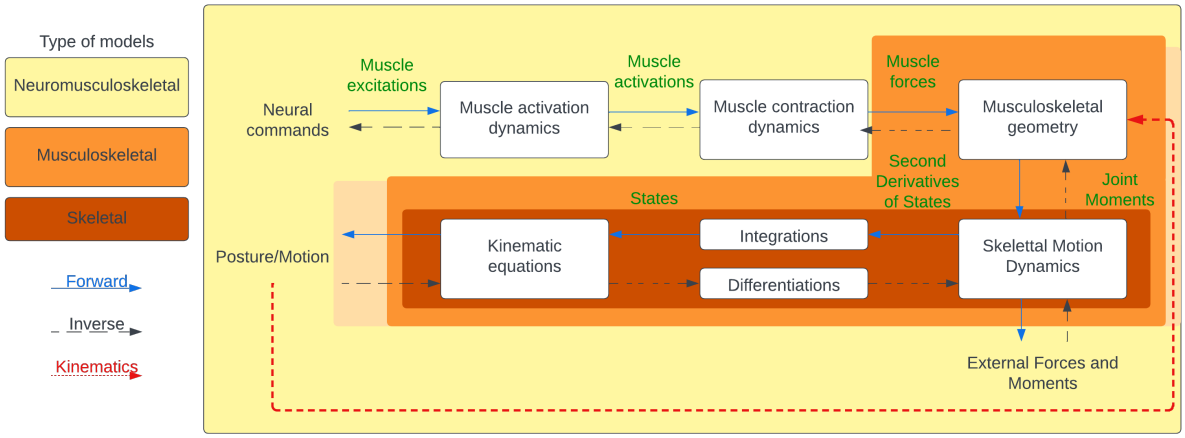

Figure 1.4: Dynamic workflow of the CNS for biomechanic analyses showing the differences between skeletal, musucloskeletal and neuromusculosketal models [17]

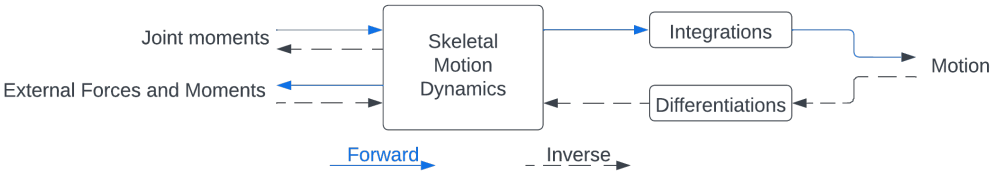

Figure 1.5: Diagram displaying the differences between forward and inverse approches for explicit dynamic formulation [17]

1.2.1 Dynamic simulation methods

Problem formulation

The human body accomplishes tasks through neural commands from the central nervous system (CNS). In biomechanical analyses, a dynamic framework is established as depicted in Fig. 1.4. This framework outlines the progression from neural commands to specific postures and inversely. The dynamic formulation can be either explicit or implicit. In explicit formulation, system dynamics are directly integrated or differentiated, while in implicit formulation, dynamics are constraint equations satisfied within optimization-based simulation.

Skeletal Models

Skeletal models serve as a starting point for understanding human gait. This category is classified based on three explicit dynamic formulations: inverse approaches, forward approaches and mixed approaches. These formulations define the core principles of human gait simulation and lay the first stone for diverse simulation solvers.

- **Inverse approaches :** Inverse approaches tackle the challenge of determining joint moments through various methods. One approach involves the use of instrumented prostheses to measure forces and moments, although this may not always be practical. The inverse dynamics method uses captured motion data and measured external forces to solve for joint torques. Nevertheless non-invasive and efficient, this method can result in unrealistic joint torques due to experimental errors. Optimization-based methods are employed to enhance results, correcting inconsistencies between kinematics and ground reaction forces.
- **Forward approaches :** The joint torques obtained from the inverse dynamics are used as inputs to estimate motion using forward skeletal motion dynamics. Three control methodologies under-actuated, fully-actuated, and kinematically-constrained are proposed to ensure stability and robustness in forward dynamic simulations. In under-actuated methodologies, the number of joint actuators is less than the number of degrees of freedom.Thus researchers focus on foot-ground contact to control degrees of freedom (DOFs). Fully-actuated methodologies consider all DOFs, incorporating nonphysical forces and moments to track captured motions. Those forces are assumed as a residual wrench who's composed of linear and rotational actuators to control the absolute DOFs of the base body. The last control methodology gain it's name from the kinematically-constrained foot-ground contact model that is imposed to provide a stable gait. This constraint give results to a fully-actuated open-chain model during the single-support phase and to an over-actuated closed-chain model when in double-support phase.
- **Mixed approaches :** combine aspects of forward and inverse dynamics to achieve more accurate gait predictions. Feedback-control methods, including the hybrid zero dynamics-based control method and the computed torque control method, use feedback to update joint torques based on data-tracking errors from forward dynamics simulations. Mixed approaches offer a bridge between the predictive nature of forward dynamics and the adaptability of feedback control.

Musculoskeletal Models

Musculoskeletal models enhance simulation accuracy by considering muscle dynamics and interactions. These models simulate muscle activations and contractions, providing a more detailed understanding of muscle contributions to gait patterns. This category includes approaches utilizing muscle activation and/or contraction dynamics.

Neuromusculoskeletal Models

Neuromusculoskeletal models extend musculoskeletal models by incorporating neural control strategies. These models integrate the neuromuscular system to simulate the interactions between neural pathways, muscles, and joints during gait. They offer a deeper insight into the complex coordination between neural signals and muscle actions.

While muscle dynamics and neuromusculoskeletal models enhance simulation fidelity, they demand complex calculations and significant computational resources. Different formulations offer trade-offs between accuracy and computational efficiency, allowing researchers

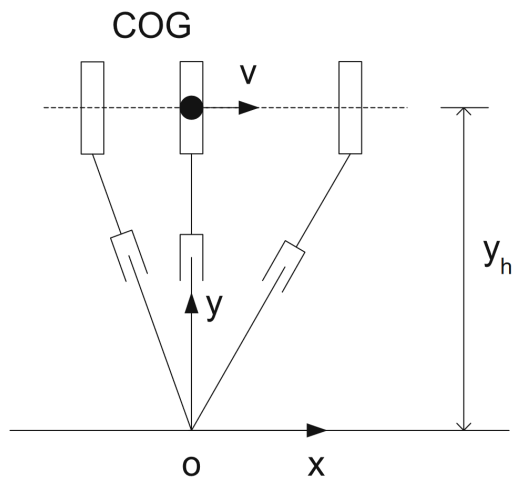

(a) Planar inverted pendulum model [18]

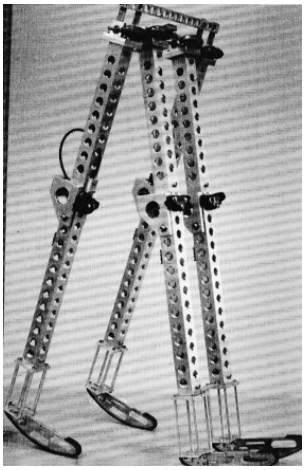

(b) McGeer's experimental passive biped [19]

Figure 1.6: Example of human gait simulation models.

to tailor simulations based on specific research goals.

In conclusion, recent advancements in predictive human gait simulation methods have led to diverse approaches in modeling, problem formulation, and simulation solvers. These approaches cater to a wide range of applications, enabling researchers to delve deeper into the complexities of human locomotion and its implications for various fields. The constant refinement of these methods continues to bridge the gap between predictive simulation and real-world gait dynamics.

1.2.2 Modeling of the human gait

Advancements in simulating human walking have introduced a range of modeling concepts that aim to replicate the natural dynamics of bipedal locomotion. This section explores three of these modeling approaches: the inverted pendulum model, passive dynamics walking, and the zero moment point (ZMP)-based method.

Inverted pendulum model

The inverted pendulum model (IPM) is a fundamental representation of walking dynamics, relying on a simple pendular exchange between potential and kinetic energy. This model (see Fig. 1.6a) serves as an initial step toward simulating walking, offering a straightforward closed-form analytical solution for the center of gravity trajectory. While the IPM provides simplicity, it lacks accurate dynamics and struggles to generate truly realistic human motion. By simplifyng the human body as a concentrated mass at the center of gravity, this model captures basic energy exchange patterns during walking but fails to capture intricate biomechanical nuances.

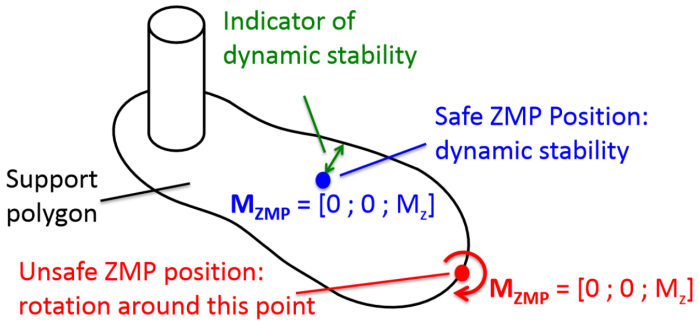

Figure 1.7: The ZMP position is the point where the net moment M_{ZMP} of inertial gravity forces has only a vertical component. The distance between the ZMP and an edge of the polygon is a good indicator to it's stability. [21]

Passive dynamics walking

Passive dynamics walking introduces a paradigm where robots emulate human-like gaits driven solely by gravity, without active control over joint angles. These walkers (see Fig. 1.6b) rely on natural pendular leg motions and angular momentum conservation to generate motion downhill, like the pendulum's swing. This approach contrasts with actively controlled robots, emphasizing energy efficiency and stability [20]. Passive dynamics walking provides insights into fundamental gait principles, such as step-length-velocity relationships and energy expenditure. Although this model lacks active control, its simplicity allows researchers to study the essence of human walking mechanics.

ZMP-based methods

Bipedal locomotion involves distinct phases defined by foot-ground contact: the single support phase with one foot in contact, and the double support phase when both feet touch the ground. For stability in static bodies, the center of mass (COM) projection onto the ground must stay within the support polygon. As bodies move, factors like linear and angular accelerations add complexity. This added complexity brings us to the Zero-Moment Point (ZMP), an evolution of COM for dynamics.

The ZMP marks the point where gravity and inertia-induced tipping moment balance out to zero. This equilibrium keeps the body stable within the polygon Fig. 1.7. Getting the ZMP close to the edge of this polygon, leads to rotation around the edge, risking a fall. ZMP-based controllers aim to maximize proximity to this edge. While ensuring dynamic stability, ZMP's criterion requires extensive local control. Even if ZMP reaches the stance foot's front edge, recovery is feasible upon the swing leg's next ground contact. Strict ZMP adherence makes the stance foot stay flat which induce a bent knee walking style, impacting efficiency, stability, and natural gait compared to humans.

Optimization-based methods

The technique of optimization-based human motion prediction serves as a prevalent computational approach for simulating and studying human movements. This method manages intricate models with numerous degrees of freedom (DOF) and can optimizes various performance metrics linked to human motion. When applied to simulate human walking, this method generates optimal motion patterns and joint force profiles while respecting essential constraints.

Control-based methods

The strength of these methods lies in their ability to sinthesize motion at inreactive rates and producing motion by using feeedbacks strategies that continuously adapt to the real world. This allows them to closely mimic actual human control systems, enabling accurate tracking, simulation, and analysis of both typical and pathological walking patterns. This holds special significance for neurological investigations of human locomotion, particularly in the diagnosis and treatment of abnormal gait conditions.

In robotics, the control-based methods enable real-time generation of walking sequences for humanoid robots, facilitating interactions with the environment and responsive task execution. Within biomechanics, control methods are harnessed to trace human movements, analyze pathological gaits, and compute muscle activations and forces. Among these approaches, the experimental-based tracking method has emerged as a powerful tool, exemplified by systems like LifeModTM, AnyBodyTM [22], and SIMMTM.

Now that the basis of today's advancement in simulating the human gait are set, the next chapter will focus on the presentation of the SIMBICON model that is used as a basis to create the controller of this thesis. The SIMBICON model can be considered as a skeletal model using control-based methods.

Chapter 2

SIMBICON model

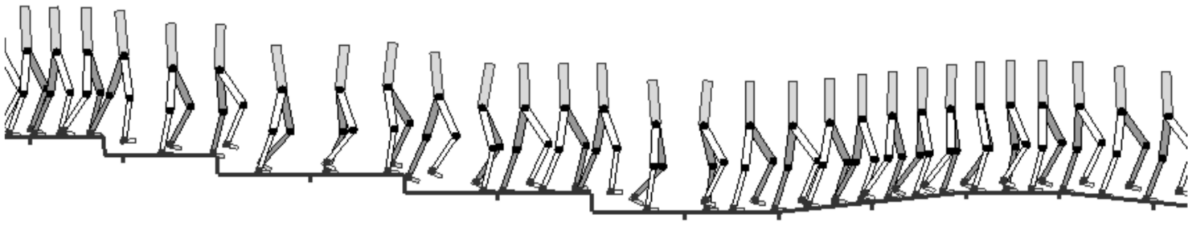

Figure 2.1: Real-time physics based character simulation of the SIMBICON framework. A single controller for a planar biped responds to unanticipated changes in terrain[23].

The **Sim**ple **Bi**ped Locomotion **Con**trol (SIMBICON) model is a control strategy designed to address the challenges presented in the previous chapter.

The starting point of the model is the use of a simple finite state machine (FSM). Each state of the FSM consists of a body pose representing the target angle with respect to their parent links for all joints of the biped. All individual joints try to reach their target angle using proportional-derivative (PD) controllers. Transitions between the states occur either after a pre-determined duration of time or after the swing foot impacts the ground.

The current FSM lacks a concept of balance, resulting in a non-robust locomotion. However, by introducing a minor set of adjustments to this design it creates a robust locomotion. Firstly, they stipulate that the torso and the hips angles are expressed in the world frame unlike the remaining links. To ensure the resulting torques are physically realizable without the use of external/virtual torques, the stance-hip torque is left as a free-variable. Then, a feedback term is incorporated to the swing hip target angle. This feedback allows the controller to adapt the future point of support of the currently swinging leg which provides the controller with balancing behaviour.

The resultant controller is applicable to both 2D and 3D bipeds and exhibit resistance against substantial pushes and variations in terrain. The SIMBICON model can generate many distinct locomotion styles through physics based forward dynamics simulations. The motion in the simulation is exclusively produced using physically viable torques, im-

plying that this approach could also extend to humanoid robots.

Despite the simple implementations of the SIMBICON model, it is able to figure out the biomechanical principles of the human locomotion while keeping kinematics results close to experimental data. Making it a good starting point to develop a simulated human gait with the goal to help in the development of a prosthetic device. In this chapter we will develop the SIMBICON balance control strategy working principles, explain how to design new controllers based on the model and finally we will talk about the pros and cons of the model in its actual form.

2.1 The balance control strategy

The balance control strategy is characterized by three elements: a finite state machine, torso and swing hip control, and balance feedback. Each of these elements is described in further detail in this section.

2.1.1 Finite state machine

The control mechanism operates using finite state machines. Each state within this framework is associated with a specific target pose, dictating the internal joint angles as depicted in Fig.2.2. In cases where the gait is symmetric, certain state pairs show left-right symmetry such as states 0 and 2, or 1 and 3. The progression from one state to another is either triggered by a passage of time, as seen in the transition from state 0 to 1, or by a foot making contact, as observed in the transition from state 1 to 2.

Should a foot contact occur before entering a state with an outgoing foot-contact triggered transition, the controller automatically bypasses that state. Within each state, the joints develop torques calculated using proportional-derivative control, denoted as :

$$\tau = K_p * (\theta_d - \theta) + K_d * \dot{\theta}$$

This control approach facilitates the movement of each joint towards its intended local angle. It is worth noting that while the prescribed poses represent the desired joint angles, they are often not fully attained in practice.

For instance, in the context of state 1 illustrated in Fig.2.2, the swing leg (left) is about to hit the ground so we could think that the targeted posture would have its swing leg extended forward. However as we can see the swing hip target angle is in flexion and not in extension as one would normally think. This design propels the swing leg in a downward motion, ultimately causing it to come into contact with the ground.

2.1.2 Torso and hip control

The stance hip and swing hip motions are managed independently, as depicted in Fig.2.3(a). For better control over the foot placement, it is necessary to detach the positioning of the swinging foot from the current pitch angle of the torso. This separation is accomplished

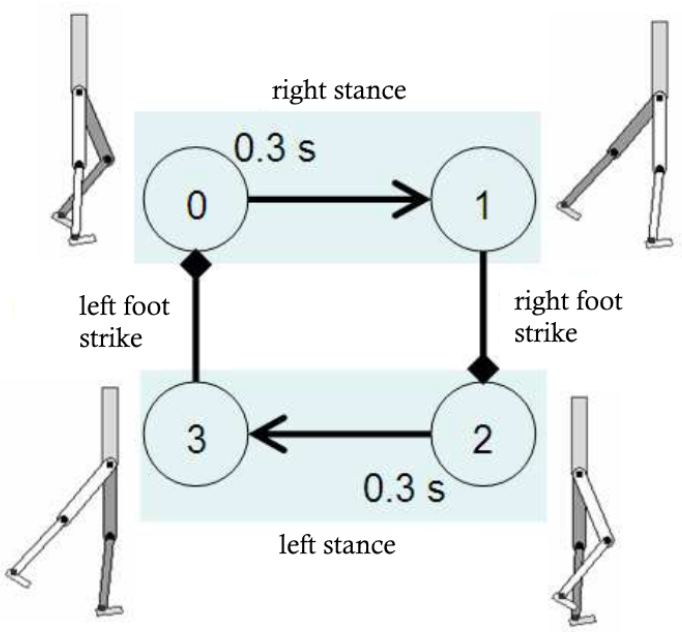

Figure 2.2: Finite state machine designed for normal walking.[23]

by regulating the motion of the swing hip with relation to the global coordinate framework. The torque acting on the swing hip, τ_B, is similarly determined by a virtual PD controller operating in the global reference frame.

There is also a prerequisite that, the virtual torques, namely τ_{torso} and τ_A, must be achievable exclusively through internal torques. This requirement mandates that the desired value of torso indeed corresponds to the net torque experienced by the torso. This is realized by computing the torque on the stance hip as:

$$\tau_A = -\tau_{torso} - \tau_B$$

2.1.3 Balance feedback

The final element of the control strategy involves implementing a balance feedback approach for adjusting the placement of the swinging foot. We utilize a feedback formula on the target angle of the swing hip represented as:

$$\theta_d = \theta_{d0} + c_d d + c_v v \tag{2.1}$$

In this equation, θ_d represents the desired angle used for PD control at any given moment. θ_{d0} stands for the preset fixed target angle outlined in the FSM. Additionally, 'd' symbolizes the horizontal distance from the stance ankle to the center of mass (COM), as depicted in Fig.2.3(b), while 'v' corresponds to the center of mass velocity. To estimate the center of mass's position and velocity, the midpoint of the hips serves as a straightforward yet effective approximation. This simplification is applicable in both two-dimensional and three-dimensional contexts.

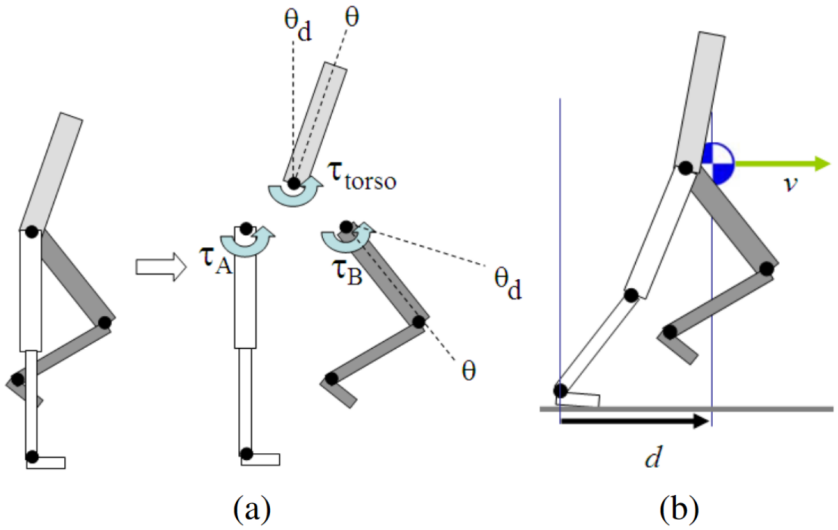

Figure 2.3: Elements of the balance control strategy: (a) Relation-ship between torso, stance-hip and swing-hip torques; (b) Center-of-mass position and velocity [23].

The feedback gain parameter c_d is important to maintain balance during slow-paced gaits or stationary stepping. For instance, consider a scenario where an in-place walking gait is desired, meaning the target velocity is zero ($v = 0$). In such a case, two potential COM positions arise: d_a at $+X$cm and d_b at $-X$cm. In the first scenario, a swift forward step is necessary, while in the second, a rapid backward step is needed to regain stability. The combined values of ('d', 'v') offer comprehensive information regarding the current phase within the gait cycle. In contrast, relying solely on 'v' provides insights solely into the current velocity error.

For 3D simulations, the balance feedback is extended to the coronal plane. But this is not discussed here as this master thesis goal stops at 2D walk modeling.

2.2 SIMBICON's basic controllers flaws

Like every other gait simulation model, SIMBICON has its own flaws. In our case despite the personal effort to adapt the SIMBICON parameters to match the kinematic of the human gait collected from in lab experiments as depict Fig.2.4. A problem could not be solved with the basic SIMBICON controller. The tibial angle w.r.t. the world frame do not pass the vertical during the swing phase as depicted on Fig.2.5b and is negative at the time of impact of the swing leg as we can see on Fig.2.5a. Effectively for ELSA to work properly, the shank of the prosthesis needs to have a θ angle greater than 0° during the swing phase. As this will lead to a proper heel impact that is primordial to lock ELSA's passive spring.

Thus there is a need to modify the base normal walk controller of the SIMBICON model in order to be able to design a controller that fills this requirement. The implementation of such a controller is described in details in the next chapter. But before presenting this

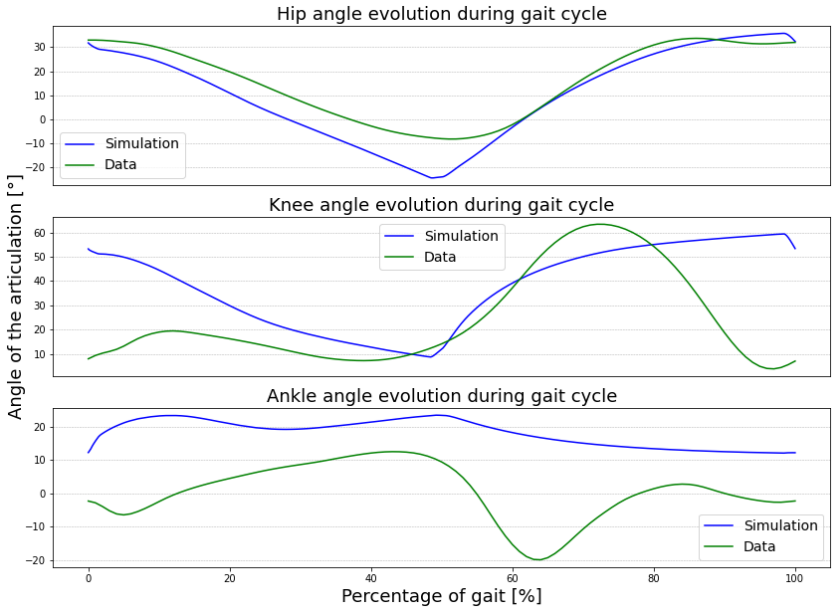

Figure 2.4: Comparison of the evolution of the angle of the hip, knee and ankle during a gait cycle between the results of the SIMBICON model and data [24]

model let's first have a quick view on how to manually design a SIMBICON controller according to its developers.

2.3 Manual design of a SIMBICON controller

Considering the controller architecture outlined before (see Section 2.1.1), there is a need for methods for determining state quantities and parameters with each state. These parameters should align with the designer of the control-system's needs. However, defining exact requirements is complex, as locomotion criteria vary (measure of style, robustness, efficiency,...). To tackle this, the developers of the SIMBICON model explored manual finite state machine design before resorting to more complex schemes. Control parameters fall into 5 different categories:

- States and state-transitions parameters.
- Balance feedback gains (c_d&c_v).
- The target poses within each state (Target angles of each articulations).
- Initial controller state
- Joint limits, torque limits, and PD-controller gains of the articulations.

State count choice reflects the level of detail that is accounted to each distinct phases of a locomotion pattern. The SIMBICON normal walk controller for instance, use four states for two symmetrical steps. Each steps has 2 states, the first raises the swing foot upward and forward for a predetermined duration, while the second propels the swing

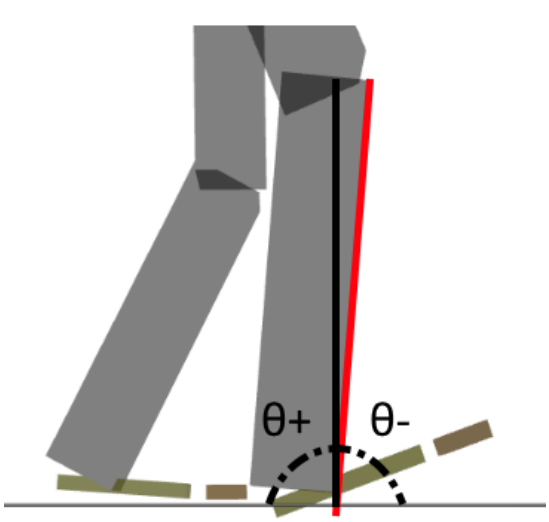

(a) Tibial angle being to small at the moment of impact.

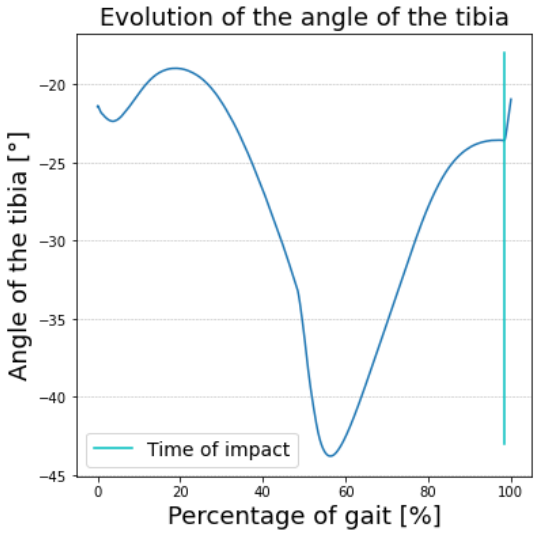

(b) Evolution of the angle of the tibia w.r.t. the world frame during a gait cycle of the SIMBICON model.

Figure 2.5: SIMBICON model flaws.

foot downward until contact with the ground is made.

The SIMBICON's developer initiate the design of controllers using the 2D biped model, which then serves as a foundation for crafting corresponding 3D controllers. A graphical user interface (GUI) that can be found on the project's web page [25], is used for interactive parameter exploration. This GUI allows users to instantly witness the effects of parameter alterations in a ongoing simulation.

In each state the parameters having the most effect on the resulting gait are the state duration Δt and the target angles for the swing hip and swing knee. As the resulting motion style heavily depends on these three parameters per state, users can readily explore their settings interactively to achieve desired motions. On the other side, balance feedbacks parameters are configured similarly accross different controllers.

These information gives us a good idea of how to manually create our own controller. However the GUI that we are talking about in this sub-section is old dated and we were not able to use it to design the controller of the next chapter.

Chapter 3

Human gait simulation

As explained in the contextualization of this research (Chapter 1), this study aims to reproduce the behavior of human gait by creating a walking biped. To achieve this goal it is first necessary to implement a digital twin of a biped. This is done using the **Robotran** program.

This chapter describes the creation and implementation of the biped. Then it describes the ground contact model that was used for the simulations and the 6 states FSM that was developed to power the biped. Finally, the results of the newly designed FSM are discussed and compared with data from in lab experiments.

3.1 Implementation of the 7-link BIPED

For reasons of simplicity and available resources, we decided to limit ourselves to the simulation of a 7-link biped in a 2D environment. The 7-link biped model developed with **Robotran**, is illustrated in Fig.3.1. The corresponding 3D model used for visualisation is illustrated in Fig.3.2a. And finally, the angles and reference conventions used in the rest of this study are depicted on Fig.3.2b.

RObotran is a multi-body dynamics simulator developped by the Multibody Research Group of the Mechatronics, Electrical Energy and Dynamic Systems division which is part of the institute of Mechanical, Material and Civil engineering of the Université Catholique de Louvain. Robotran was designed in the purpose of analysing mechanical systems using a symbolic approach.

In Fig.3.1, one can see the different bodies created to implement the biped. At the top, the HAT (Head Arms Trunk) is linked to the ground through 3 degrees of freedom (DOF): x-axis and z-axis translation and y-axis rotation (the link q9 corresponding to an y-axis translation) is not counted as a DOF as it is only there to move laterally the biped and it is imposed to a fixed quantity through the whole simulation. From the HAT, the two hips (Left_thigh & Right_thigh) are connected with a rotational DOF around the y-axis. Then for each leg, the following element (Shanks, Foot and Toes) are connected to the previous one with a rotational DOF around the y-axis. It is important to highlight that their is no translation in the y-axis and no rotation around the z-axis to simplify the

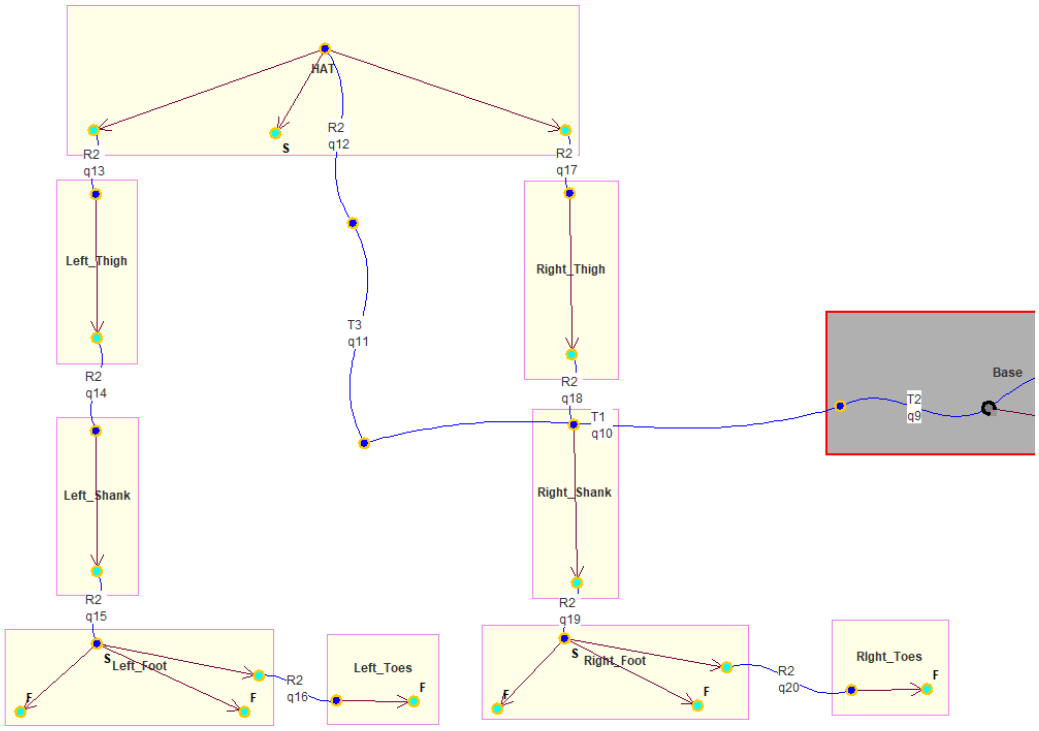

Figure 3.1: 7-link biped model via Robotran MBsysPad.

model, i.e we will be working in the sagittal plane.

The 7-link planar biped anatomical values (segment length, mass and inertia) are based on Winter's data. Effectively, given that the anatomical dimensions of the walker profoundly influence its dynamics and ballistics, it is crucial that our walker closely aligns with the anatomical characteristics of the individuals from whom the data used for comparison for this thesis were gathered from.

However the data that we compare our results to [24] only indicates the mean height (1.71 [m]) and the mean weight (68.5[kg]) of the patients that participated to the experiments. Hence the biped's anatomy was built following Winter's work [26].

Segment	Segment length	Segment weight
Hat	0.19	0.678
Thigh	0.245	0.1
Leg	0.246	0.0465
Foot	0.152	0.0145

Segment	Proximal COM	α
Hat	1.142	0.903
Thigh	0.433	0.323
Leg	0.433	0.302
Foot	0.5	0.475

Table 3.1: Tables containing the values required to calculate the values inside Table3.2. Values of this table were calculated thanks to Fig.A.1 and TableA.2. Left table's values are related to total body height/weight. Right table's values are related to segment total length.

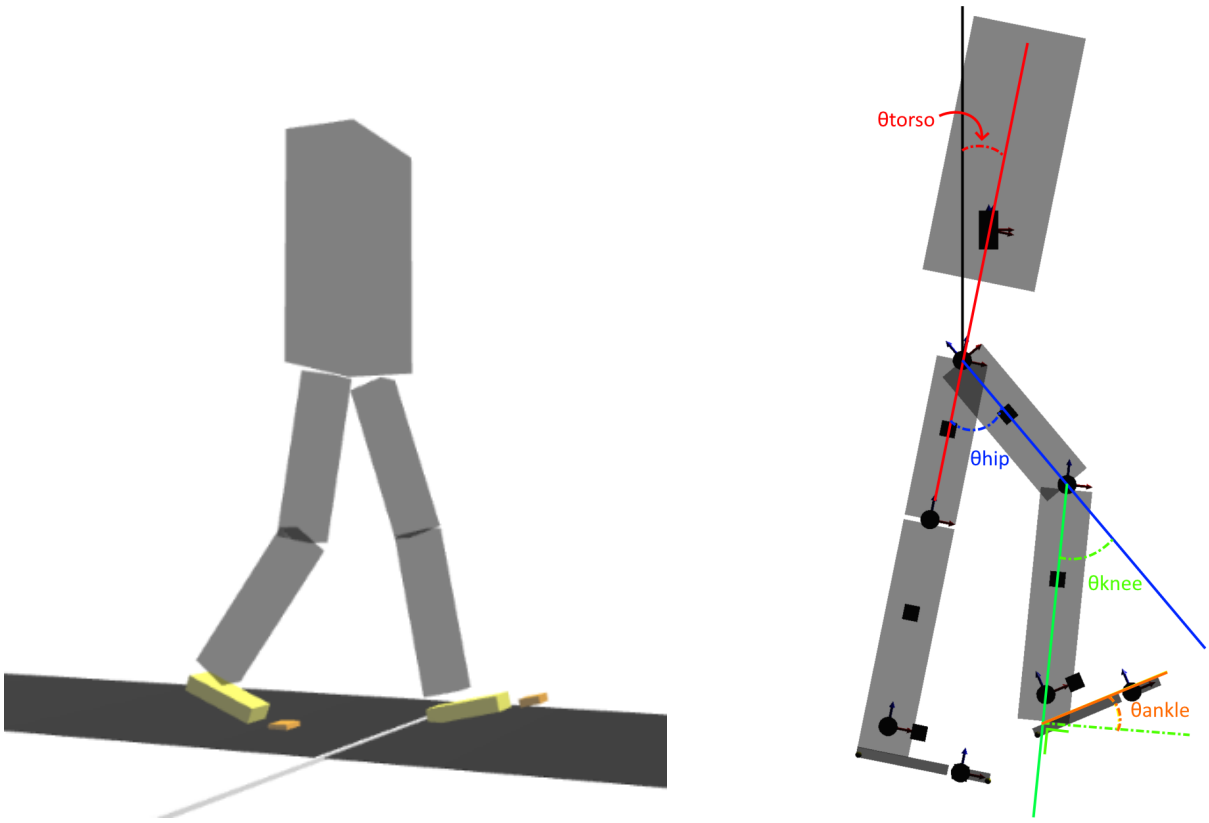

(a) 3D graphical representation of the 7-links biped.

(b) Angles of reference.

Figure 3.2: 7-link biped presentation.

Segment	Length[m]	Weight[kg]	COM [m]	Inertia $[kg * m^2]$
HAT	0.3249	46.443	0.37104	3.99756
Thigh	0.41895	6.85	0.18141	0.12544
Leg	0.42066	3.18525	0.18215	0.05141
Foot	0.25992	0.99325	0.12996	0.01514

Table 3.2: Table of the needed values for the MBsysPad model of the Robotran program.

With the values of Table 3.1. We were able to establish the values of Table 3.2. The length, mass and COM of the segments were calculated directly from the values of Table 3.1. And the inertia of the segments about their center of mass were calculated using the following equation:

$$I_o = m * (l * \alpha) \tag{3.1}$$

Where, I_o stands for the moment of inertia about it's center of mass, m is the mass of the segment, l is the length of the segment and α is the Radius of Gyration related to the segment length.

3.2 Ground contact model

The ground contact model is composed of two forces a normal one being perpendicular to the ground and a friction one being parallel to the ground. These forces are applied to the biped through six contact points, three on each feet being situated at the back of the foot, the front of the foot and the toes as it is shown on the figure on the right. The contact forces are only calculated and applied to a point once the point in question is lower than the level of the ground. All the parameters of the ground contact model are available in Tab.3.3. It is important to note that the same ground contact model was used for the simulation of the SIMBICON model of the previous chapter.

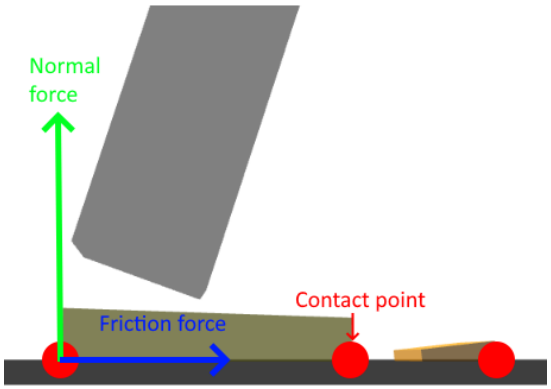

Figure 3.3: Normal force, friction force and contact points of the ground contact model.

3.2.1 Normal force

The normal force is modelled by a spring-damper equation. In this model, the first term on the right-hand side is referred to as the elastic force component (spring) and the second term account for the energy dissipation during the contact event (damper).

$$F_N = K\delta + D\dot{\delta} \tag{3.2}$$

K	D	μ	K_v
$1.0e^5$	$6.0e^3$	0.65	0.725

Table 3.3: Ground contact parameters

Where F_N is the contact normal force, δ is the relative penetration and $\dot{\delta}$ denotes the relative normal contact velocity. K and D are respectively the generalized stiffness parameter and the damping coefficient.

3.2.2 Friction force

The friction force is modelled by the Integrated Coulomb and viscous model [27].

$$F_f = \begin{cases} min(F_c, K_v\dot{x}) & if\dot{x} \geq 0 \\ max(-F_c, K_v\dot{x}) & if\dot{x} < 0 \end{cases} \quad (3.3)$$

Where F_F is the friction force, K_v is the viscous coefficient, $\dot{x}$ is the sliding speed and :

$$F_c = \mu * F_N \quad (3.4)$$

stands for the Coulomb friction force where μ is the friction coefficient and F_N is the normal force. The figure on the right shows the evolution of the friction force.

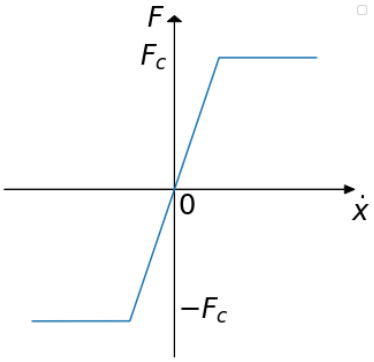

Figure 3.4: Evolution of the friction force as a function of sliding speed.

3.3 6 states FSM SIMBICON based controller

The controller is based onto SIMBICON's controller architecture, it has the same way of handling torso & hip control and the same balance feedback strategy. However instead of having 4 states for simple walking, 2 states were added to the FSM for an increased level of detail of the human gait. A scheme of the 6 states of the FSM with the target pose of each state is depicted on Fig.3.5.

The controller have three transition conditions depending on the state he is currently in:

- **Stance hip angle transition:** (States 0 & 3) The controller waits for the stance hip to reach a certain angle. As there's no control on the stance hip (see Section2.1.2) adding a state transition that depends on the angle of the stance hip brings a sort of control on the stance hip. During this state, the previously stance leg becomes the swing leg. This leg must now pass in front of the other in order to make contact with the ground again in a forward direction. To do so, the thigh and knee of the swing leg will have a moment of flexion until the angle of the thigh of the supporting leg passes the vertical.

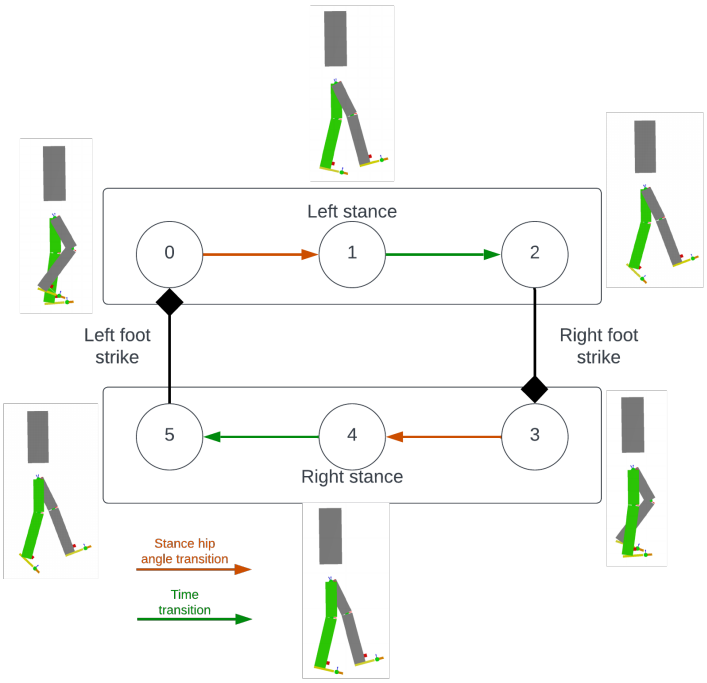

Figure 3.5: 6 states finite state machine designed for realistic normal walking. Green represents the stance leg and grey represents the swing leg.

- **Time based transition:** (States 1 & 4) Just like in the SIMBICON controller, in this states the controller just wait a certain amount of time. When this states start, the stance hip angle just passed the vertical. Which induce that the biped is now going to fall forward since it's stance foot is behind his center of gravity and his swing hip is contracted forward. This state can be seen as the state where the potential energy is transformed into kinetic energy. As we can see on Fig.3.5. During this state the swinging knee will extend himself to prepare for the next impact.
- **Impact based transition:** (States 2 & 5) In this state, the controller waits for the swing foot to touch the ground before switching to the next state. During this state the stance ankle targets a plantar flexion position. This will propel the biped forward to ensure that it has enough kinetic energy to allow the future supporting thigh to pass the transition angle.

The target angles of the controller can be found in A.3.

3.4 Results

This section presents the results obtained from the controller designed in this chapter, which serve as a validation of the model for subsequent chapters. All the following graphs in this research with an x axis representing the percentage of the gait cycle starts with the stance phase followed by the swing phase around 50%.

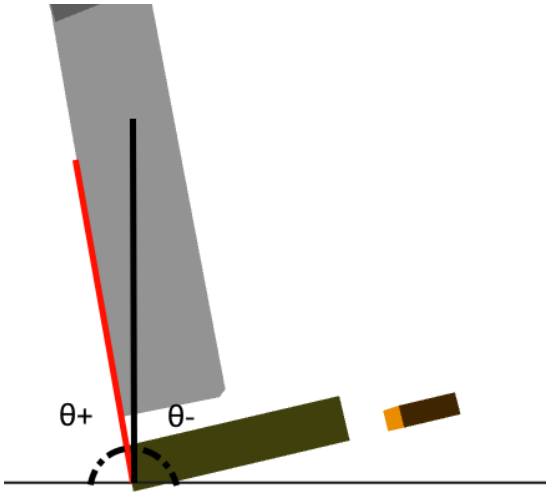

(a) New tibial angle at the moment of impact.

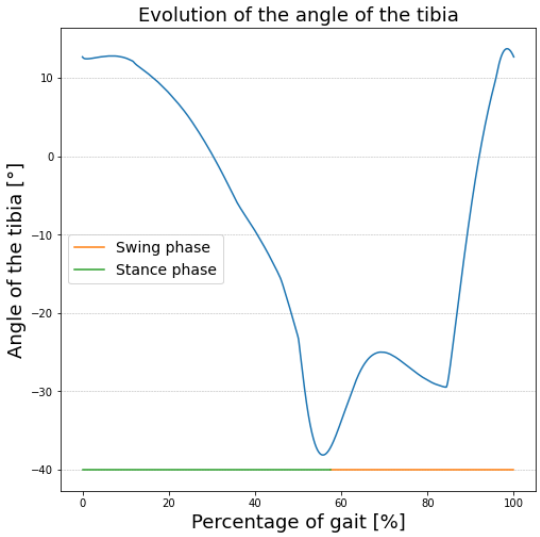

(b) Evolution of the angle of the tibia w.r.t. the world frame during a gait cycle of the developed model.

Figure 3.6: Validation of the controller's objective

3.4.1 Kinematic results

The newly designed controller has successfully achieved its intended goal. Fig.3.6b illustrates the achieved tibial angle during the swing phase, showing positive angles and a positive angle at the moment of impact (Fig.3.6a).

A comparison of hip, knee, and ankle angles between the simulation and experimental data is shown in Fig.3.7. The simulation closely matches the data[24], with minor deviations. With the exception of the ankle angles for the swing phase of the graph (right part).

The Tab.3.4 compares the spatio-temporal parameters of the simulation with the experimental data. As one can see, the simulated walker is a bit slower than the results of experimental data. This results in a slower cadence and smaller steps. Moreover, the stance time is also slightly reduced.

Discussion

Hip and knee angles values of the simulation are close to the data. It is still noticeable that the hip of the simulation is one step ahead for the second part of the graph corresponding to the swinging part. One can also see that the flexion of the knee starts earlier and last longer in the simulation than in the experimental data.

For the ankle, the stance phase values of the simulation match the data however this is

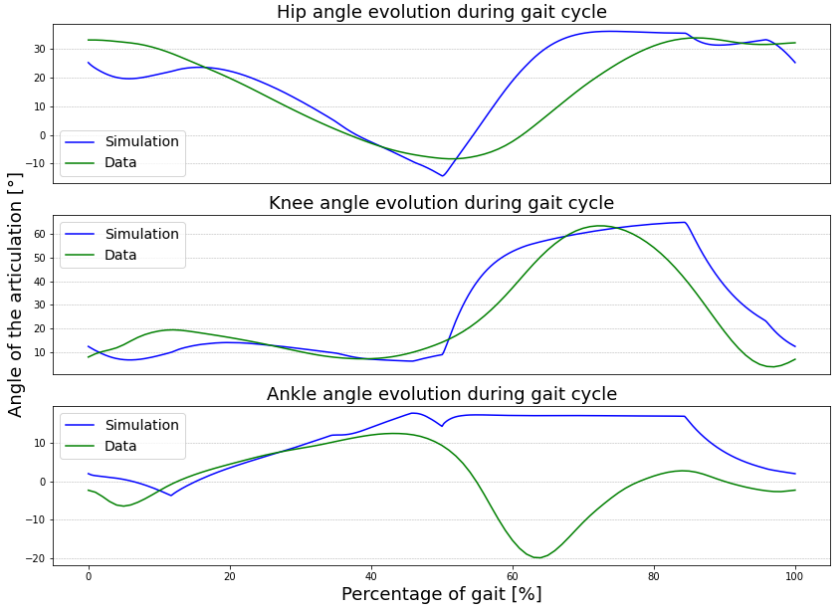

Figure 3.7: Comparison of the evolution of the angle of the hip, knee and ankle during a gait cycle between the results of the simulation and experimental data [24]

Spatio-temporal parameter	Data	Simulation
Gait speed/BH [%BH s^{-1}]	71.4	50.1
Cadence [steps min^{-1}]	110	91
Stride length/BH[%]	77.8	63
Stance time [% of gait cycle]	63	57
Double support time [%]	13	7

Table 3.4: Comparison of the spatio-temporal parameters of the simulation with the ones of the data [24]

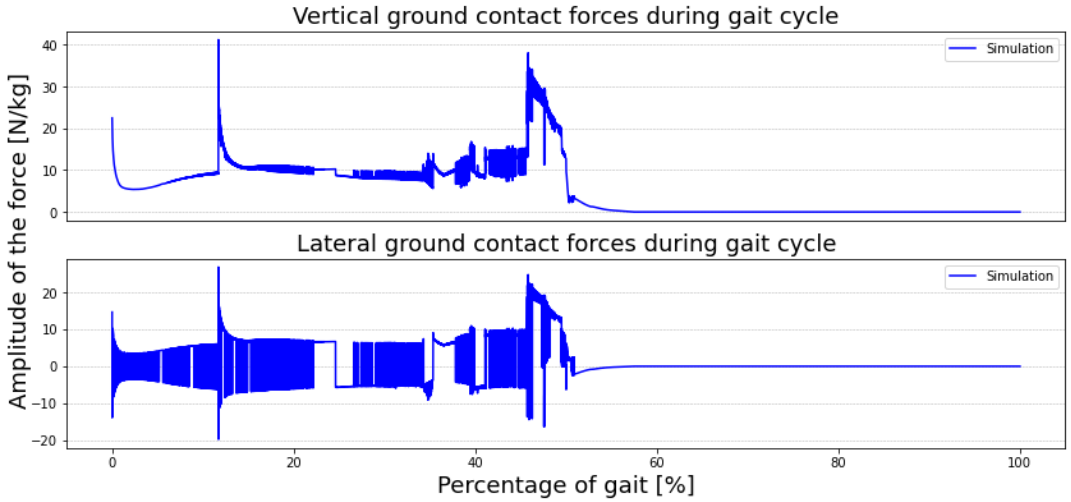

Figure 3.8: Vertical & lateral forces normalised to body weight applied to one foot during a full gait cycle.

not the case for the swing phase. This is due to the fact that if the ankle goes in plantar flexion during the swing period, there's a chance that it touches the ground which makes the biped falls. This is why the ankle target angles have been designed to stay in dorsiflexion during the swing period to avoid this problem..

3.4.2 Dynamic results

For the dynamic results, the ground reaction forces and the torque applied to each joints are depicted on Fig.3.8 & Fig.3.9. As one can see both of these diagram's data have been normalized for total body weight.

Discussion

The contact forces applied to the feet of the biped are unreal effectively, according to [28] the maximum value reached for the force should be around 120% of the walker's weight. Which should lead us to peaks around 12 [N/kg]. The reasons why such big forces are recorded couldn't be explained. Lateral forces are not real either; in fact, you can see them being applied once in the forward direction and then in the opposite direction. This is why we think that a redesign of the contact model would be interesting for future work. However despite the strange results observed in these graphs we did not notice any abnormalities during the simulations. Effectively the spike of the forces are very brief which does not impact the model too much.

The torque applied on the biped's joints are not very relevant neither, the torques also have the huge spike just as the contact force have. However once again as these torques are very short in time, they do not have a huge impact on the simulation.

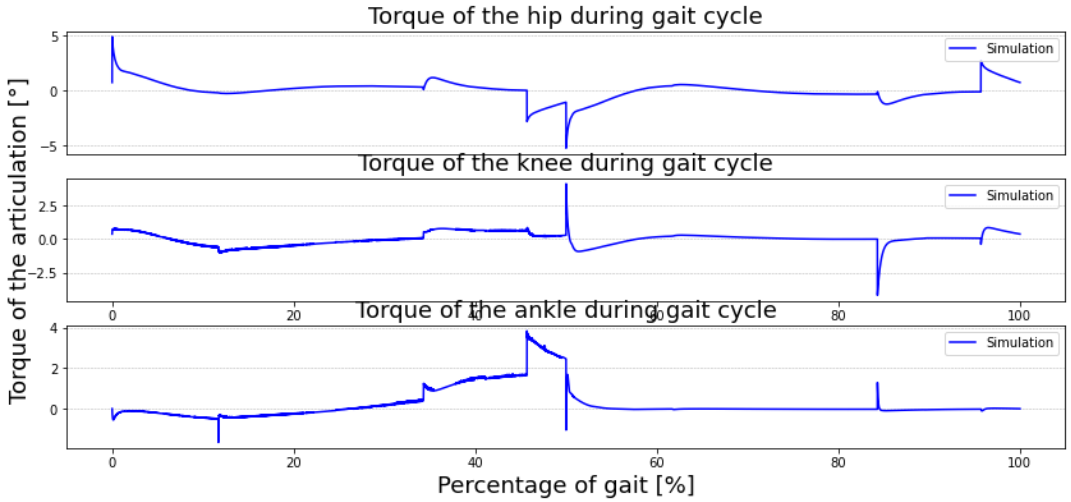

Figure 3.9: Torques applied by the controller to hip, knee and ankle normalised to body weight during a full gait cycle.

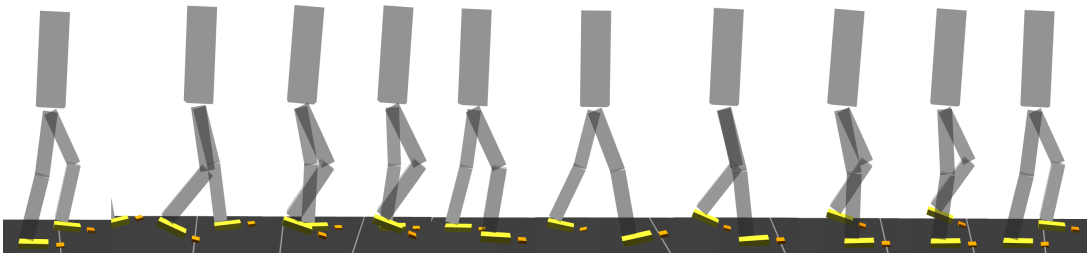

Figure 3.10: Visualisation of the posture of the biped when momentary force are applied from left to right 0% to 90%

3.4.3 Robustness test

In this section we will explore the robustness of the designed controller. Six tests were carried out to assess the robustness of the controller presented in this chapter.

First, a force in the direction of travel was applied at the HAT's COM, then a force in the opposite direction to travel was applied at the same point. This was followed by 2 constant-force tests once again applied a HAT's COM one in the direction of travel (forward) and the other one in the opposite direction (backward). Finally, 2 other tests were carried out, one on an uphill slope and the other on a downhill slope. All results shown in this section are the maximum perurbations the controller can support.

Momentary force tests

In these tests, a force was applied to the COM of the HAT during 0.1 [s], the test is performed at 10 distinct moment of the gait cycle respectively 0%,10%,20%,...,90%. The position the biped have at the beginning of each push can be visualised on Fig.3.10.

Time of application [% gait cycle]	0	10	20	30	40	50	60	70	80	90	Mean [N]
Forward max force [N]	750	425	325	400	700	700	425	325	400	675	507.5
Backward max force [N]	-50	-50	-50	-80	-80	-50	-50	-50	-80	-80	-63

Table 3.5: Maximum force withstanded by the controller before falling.

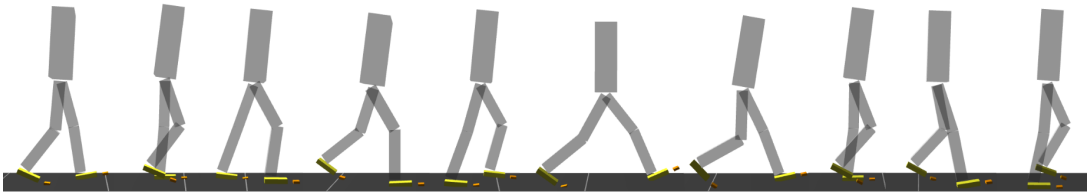

Figure 3.11: Simulation of a recovery after a push of 700[N] during 0.1[s] in the forward direction.

The maximum forces the controller can withstand are available in Tab.3.5.

Fig.3.11 shows the evolution of a recovery of the controller after a forward push. Whereas Fig.3.12 shows the evolution of a fall due to an important force in the forward direction. In this case, the fall is due to an impact of the swinging foot after take off. This early impact (1st) on the left leg leads to a destabilization of the controller which leads to an even earlier impact (2nd) on the next step. Which ultimately leads to a fall.

Finally, Fig.3.13 shows the evolution of a fall due to force applied in the backward direction. In this scenario, the fall is because the swing foot will pass over the ground without making contact (blue arrow) in the state 2 (or 5) leading to an immediate fall of the biped.

Continuous force tests

The continuous force tests consist of a constant force applied during 10 [s]. In the forward direction, the controller is able to withstand a force of 40[N]. In the opposite direction it is only able to withstand a force of 6.5 [N].

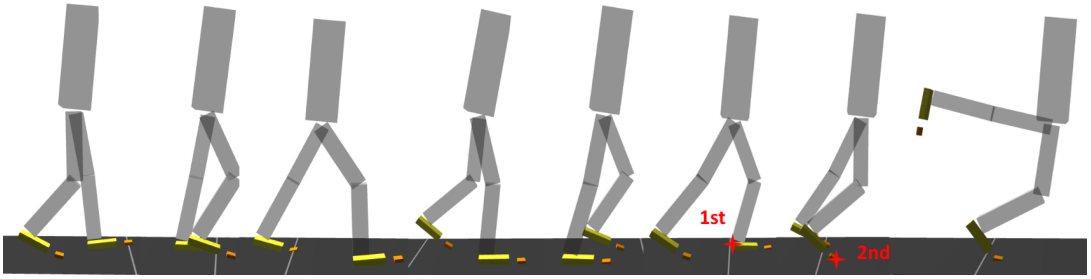

Figure 3.12: Simulation of a fall after a push of 800 [N] during 0.1[s] in the forward direction.

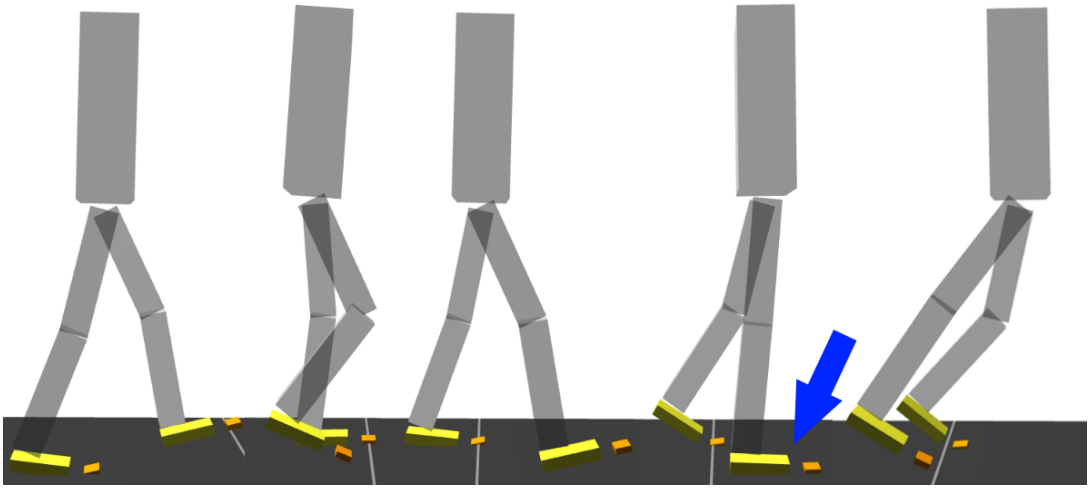

Figure 3.13: Simulation of a fall after a push of 70[N] during 0.1[s] in the backward direction.

Inclined ground tests

The inclined ground tests are very disappointing. The controller is not able to climb the smallest climb even a climb of 1°would lead to a fall. For descents, the maximum amplitude achieved is of 1.5°.

Discussion

Two important things are noticeable in those results. First of all we can see that the maximum force depends on when the force is applied to the biped. And secondly as expected, we can observe a symmetric pattern between the first 50% and the second ones corresponding to the symmetry of the walking pattern.

3.5 Conclusion

In conclusion the goal the controller was designed for was achieved, the tibial angle at impact is now greater than 0°and the hips, knees and ankles angles are closer to the ones of experimental data.

However this was not free as the controller lost a lot of its robustness compared to the basic SIMBICON controller. Effectively the SIMBICON controller is able to withstand pushes of 600[N] forward and 500[N] backward at any moment of the gait which is twice the amount the new controller can withstand in the forward direction and ten times the amount in the backward direction. Moreover where the SIMBICON controller can climb slopes of ±6° the new one can only withstand down slopes of 1.5° and cannot climb up slope. No data was given for continuous force applied to the biped for SIMBICON so no comparison is available.

We believe that this loss of robustness is due to a closer match to the kinematic of data

experiment. e.g. the feet are now closer to the ground during the swing phase which is a problem for up slope walking. Where as the SIMBICON controller had his feet ways higher during the swing phase which allows him to not touch the ground until the swinging leg is in front of the stance leg.

Due to this less of robustness, it is essential to design a new controller to restore the biped's ability to walk on slopes. The next chapter is dedicated to the creation, tests and discussion of such a controller.

Chapter 4

Adapted controller for slopes

As explained in the previous section, due to the controller's modification to approximate human walking, it is no longer able to walk on slopes. This section focuses on the changes made to the controller to enable it to regain this ability. It is important to note that from this point on, the controllers have specific tasks (e.g. the controller designed for down-slope walking is not able to walk on flat ground). This is quite logical as the slope and the inclination of the slope does influence the human gait[29]. It is therefore necessary to improve the structure of the simbicon model to enable it to switch between the different "modes".

This chapter begins by discussing the modifications made to the controller. Then it focuses on the results obtained by this newly designed controller and compare them to data collected from in lab experiments[29].

4.1 Modification of the controller's structure

For the controller to be able to walk on slopes, it is necessary to modify the target angles of its states. This is why a new variable has been implemented in the controller: the mode variable. This will enable the controller to change the target angles of each of its articulations according to the mode it is currently in.

The controller_mode_handler function (Fig.4.1), uses the position of the center of mass of the biped to check if it is currently above a flat ground or a slope. Once the ground under the center of mass changes, the function automatically switch the mode of the controller resulting in different target angles for each joint of the biped.

4.2 Implementation of the slope controllers

The mode only differ between one another in the target angles that are set for each state. Changes made to the target angles are available in TableA.3.

As we can see, the first three lines of the table shows the parameters of the controller for flat ground and slopes. The squares in light orange shows the parameters that are

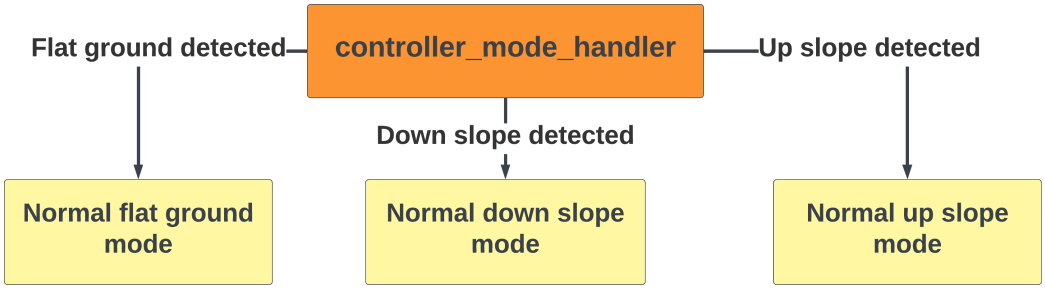

Figure 4.1: Diagram showing how the simbicon controller hangles the mode parameters to set the angles

modified. For example, we can see that the Sw Hip 0 of the up slope controller is bigger than that of the normal controller, which is perfectly logical, since more thigh flexion is required when climbing a slope.

To obtain the parameters, trial error method with the objective to match data obtained from in lab experiment was used. Finally leading to these parameters.

4.3 Results

4.3.1 Kinematic results

A comparison of hip, knee and ankle angles between the simulation and experimental data is shown in Fig.4.2 for the down slope controller and on Fig.4.3 for the up slope controller.

Discussion

As we can see, the hip and the knee match quite well the angles obtained by the data, however the ankle angle is now ways bigger than the angle obtained by experimental data.
We believe this is caused by the little differences in the hip and knee's kinematic and that the ankle angles suffer from these differences just like the SIMBICON model did. Foe the swing part of the angle the off set is because of the same reasons explained earlier in this research.

4.3.2 Robustness test

The same robustness test were applied to the controller to assess it's ability to withstand perturbations.

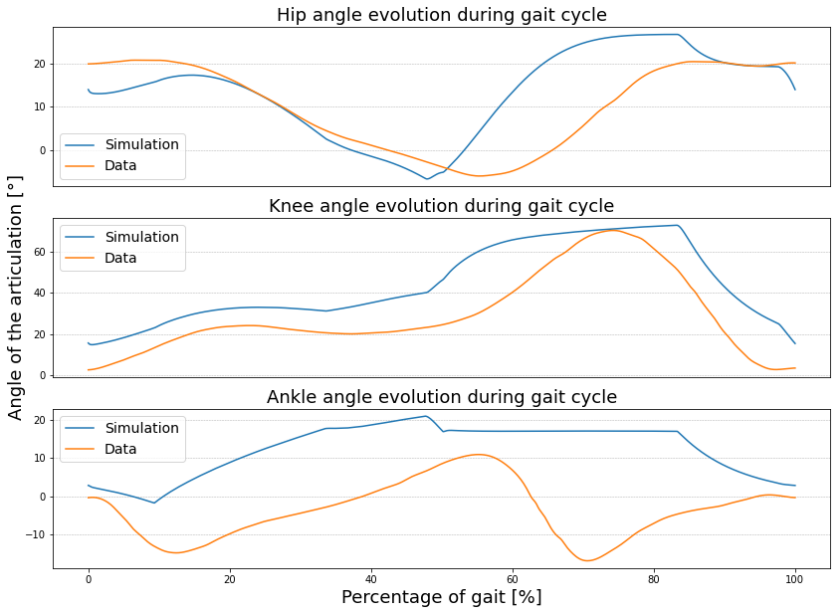

Figure 4.2: Comparison of the evolution of the angle of the hip, knee and ankle during a gait cycle on inclined down slope between the results of the simulation and experimental data [29]

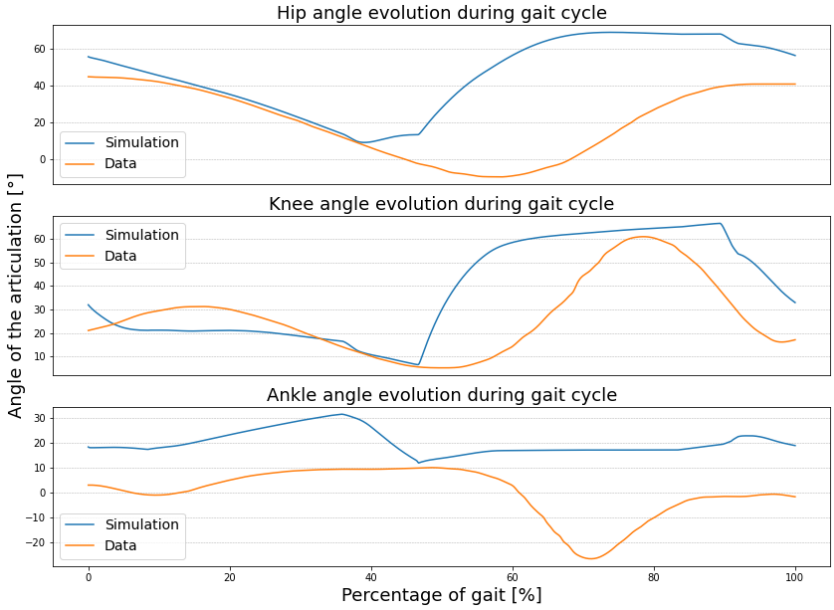

Figure 4.3: Comparison of the evolution of the angle of the hip, knee and ankle during a gait cycle on inclined up slope between the results of the simulation and experimental data [29]

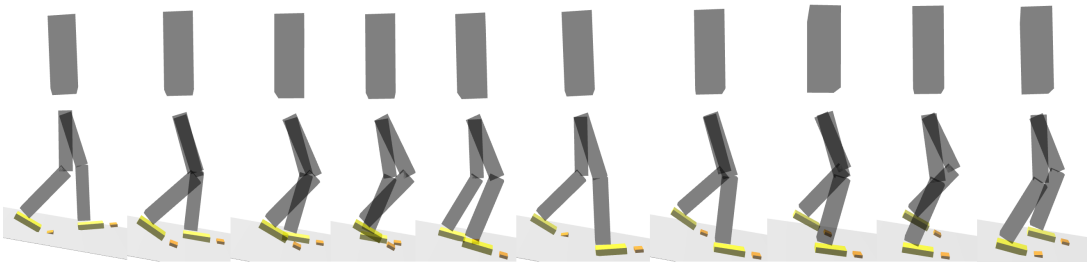

Figure 4.4: Visualisation of the posture of the biped when momentary force are applied from left to right 0% to 90%

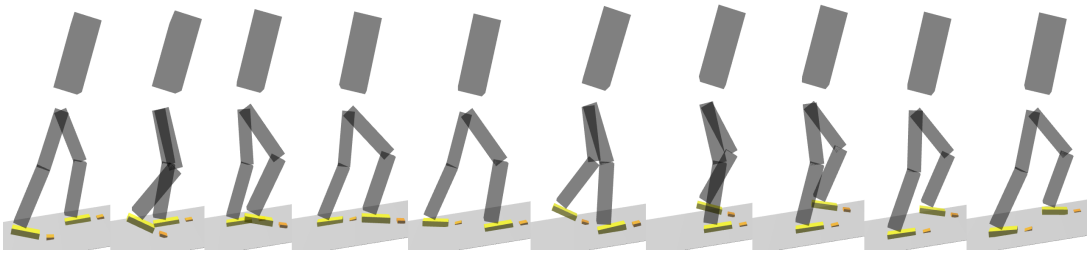

Figure 4.5: Visualisation of the posture of the biped when momentary force are applied from left to right 0% to 90%

Momentary force

The maximum momentary force the controller can withstand are available in Tab.4.1. The position the biped have at the beginning of each push can be visualised on Fig.4.4 & 4.5.

Continous force

The continuous force tests gave the following results, for the down slope controller, the maximal forward force is 50[N] and the backward force is 5[N]. For the up slope controller, the maximum forward force is 25[N] and the maximum backward force is 15 [N]

Slope variations test

The slope variations tests gave the following results for the down slope controller the maximum variations of the slope are +1/-1.5[°]. For the up slope controller the maximum

	Time of application [% gait cycle]	0	10	20	30	40	50	60	70	80	90	Mean [N]
DS	Forward max force [N]	1250	1100	1000	950	1200	1300	1100	1000	1250	1000	1115
DS	Backward max force [N]	-250	-350	-525	-125	-175	-225	-325	-450	-175	-125	-260
US	Forward max force [N]	225	250	250	250	350	375	225	100	100	150	227.5
US	Backward max force [N]	-250	-350	-525	-125	-175	-225	-325	-450	-175	-125	-272.5

Table 4.1: Maximum momentary force withstanded by the controller before falling. DS stands for down slope and US stands for up slope.

variations are +0.15/-18[°].

Discussion

By comparing the results of this section with the results of Section 3.4.3 of the previous chapter, we can assess that:

The controller designed for down slope walking is more robust to pushes than the controller designed for flat ground except for continuous forward force. And it also resist slightly better to slope variation than the original one did.

The controller designed for up slope walking on the other side is on average two times less robust to forward push . However it is three times sturdier to backward pushes. The same tendency is observed with the results of continuous pushes. And finally the controller designed for up slope walking was able to withstand an astonishing -18° down slope variations making it able to walk down slope but can only withstand a +0.15° positive variation. We can thus asses that due to the inclination of it's torso, the up slope controller exchanges it's robustness to forward pushes for robustness to backward pushes. The same assessment can be done for slope variations.

4.4 Conclusion

In conclusion,the controllers designed for slope does not reproduce the kinematic of data experiments as well as the flat ground controller did. But these results confirmed our supposition made in the previous chapter as the controller designed for slopes have better robustness results than the one on flat ground. Effectively the down slope controller is able to withstand a push of 1300[N] in the forward direction and the up slope controller is able to withstand a slope variation of -18°.

Chapter 5

Adapted passive prosthesis controller

In this chapter, we will address the changes made to the controller in order to enable it to walk with a prosthesis. Due to the lack of robustness of the controller, it is not capable of walking with a passive prosthesis, as it no longer has control over the amputated ankle, which prevents it from performing the maneuver explained in section 3.4.1.

Therefore, it is necessary to once again modify its parameters so that it can walk with a passive prosthesis. This chapter begins with an explanation of how the passive prosthesis was implemented in the simulation. Then the modifications brought to the controller are presented. Finally the results are compared with the results of the previous chapter.

5.1 Implementation of the passive prosthesis

The passive prosthesis implementation is quite strait forward, the torque applied at the ankle of the passive prosthesis is simply replaced by a spiral spring-damper with a resting position at 0°. But in preparation for the ultimate goal of this research which is to replace this passive prosthesis by ELSA prosthesis. The digital spiral spring was implemented to only be active when the prosthesis is in dorsiflexion just like ELSA.

5.2 Implementation of the adapted controller

The need to adjust the target angles depending on a new condition stands again. This time it depends on whether the biped is wearing a prosthesis or not. It is why, just like in the previous chapter, a new variable has been implemented to allow the controller to know whether it has a foot prosthesis or not.

Fig.5.1 illustrates the expansion of the controller's decision tree to allocate the correct target angles in function of the situation it is currently in. The selection of target angles based on states, modes, and whether it is wearing a prosthesis or not is handled within a single function. However, the change of state and mode are managed by separate functions. The fact that the biped has a prosthesis or not is initialised at the start of the program.

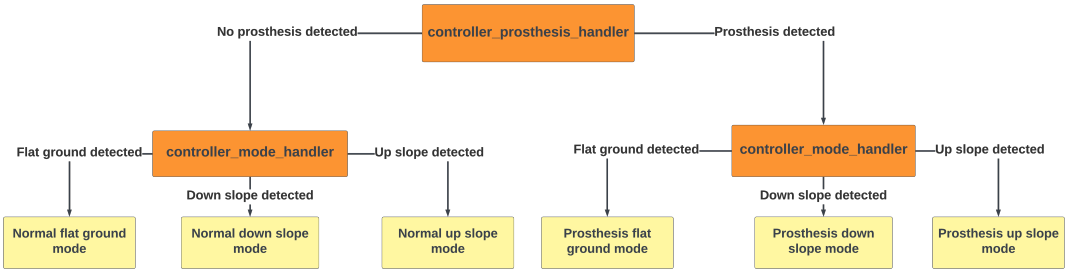

Figure 5.1: Diagram showing how the simbicon controller handles the mode and prosthesis parameters to set the target angles.

Table A.3 references the adjusted angles of the controller. This time, 2 colors are used to best highlight the modifications made to the controller. The light yellow distinguishes the changes made for the controller with a prosthesis on flat ground compared to the controller without a prosthesis on flat ground. Then, the red color distinguishes the changes made for the controllers with a prosthesis on inclined surfaces compared to the controller with a prosthesis on flat ground. Finally we can observe that two lines are dedicated to the controllers of prosthesis. This is done to differentiate the sound ankle and the prosthesis ankle. Effectively to simplify the code, the passive prosthesis case is handled by the controller like if it was a sound ankle with a target angle always equal to 0.

5.3 Results on flat ground

5.3.1 Kinematic results

A comparison of hip, knee and ankle angles between the simulations of the controllers designed for healthy biped and the controller designed in this chapter is shown in Fig.5.2.

Discussion

As can be seen in the graphs, the angles of the thigh and knee of the biped wearing a prosthesis closely follow the angles of the biped without a prosthesis during the stance phase. However, during the swing phase the angles are higher ($\approx +20°$). This is due to the fact that the ankle's angle is much lower (plantar flexion). Therefore, the biped needs to bend the knees and thighs much more during the prosthesis swing to ensure that the prosthesis toes does not touch the ground.

5.3.2 Dynamic results

Fig.5.3 compare the torque of the sound ankle and the torque generated by the passive prosthesis.

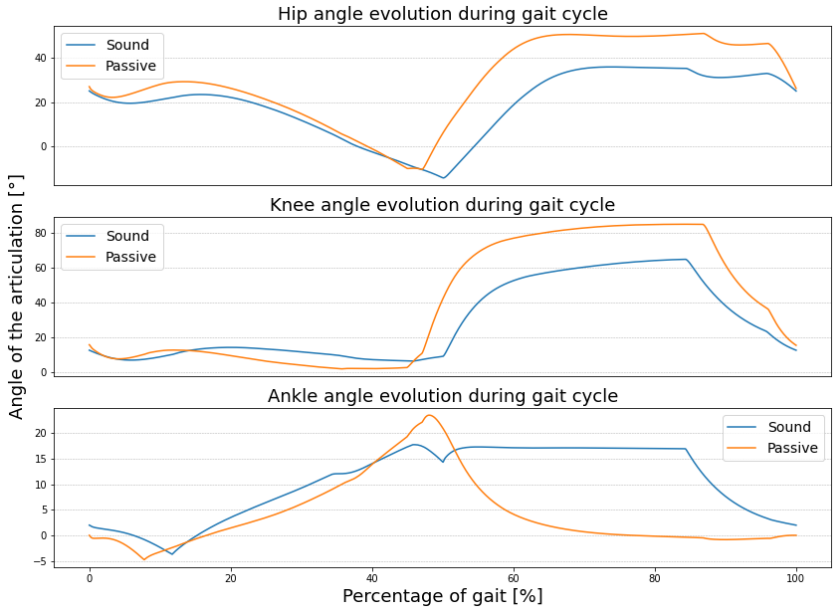

Figure 5.2: Evolution of the angle of the hip, knee and ankle during a gait cycle on flat ground. Comparison between the results of the simulation of the sound biped and the passive prosthesis amputated biped.

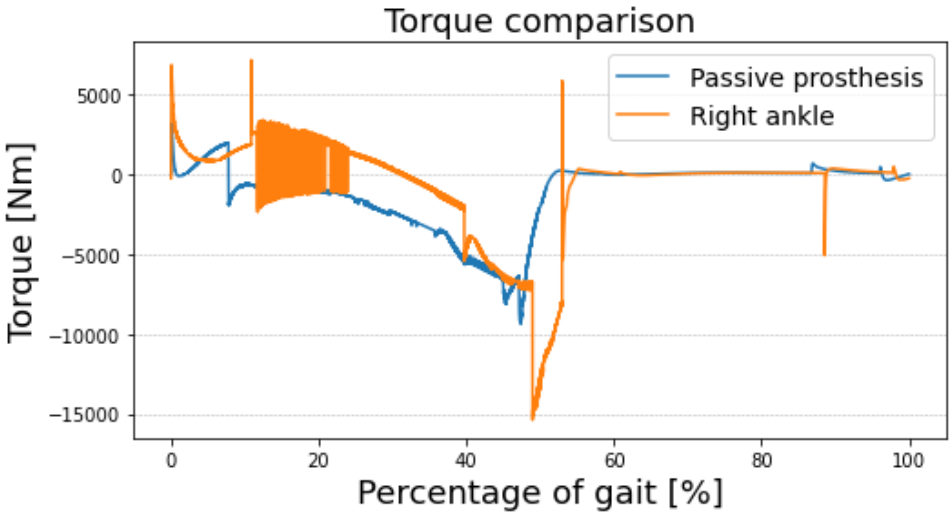

Figure 5.3: Graph of the torque generated by the passive prosthesis versus the torque generated by the controller on the sound ankle.

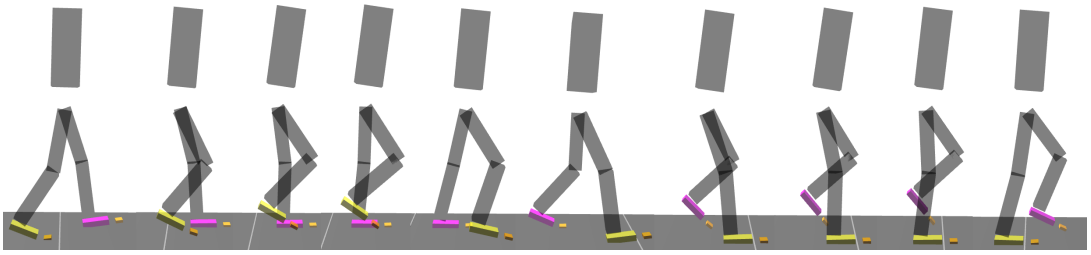

Figure 5.4: Visualisation of the posture of the biped when momentary force are applied from left to right 0% to 90%. The pink foot is the passive prosthesis.

Time of application [% gait cycle]	0	10	20	30	40	50	60	70	80	90	Mean [N]
Forward max force [N]	450	400	300	350	475	600	375	275	325	450	400
Backward max force [N]	-75	-100	-100	-50	-50	-75	-100	-100	-125	-75	-85

Table 5.1: Maximum force withstanded by the controller before falling.

Discussion

As can be seen in the graph, the passive prosthesis generates a slightly higher torque than that generated by the healthy ankle during most of the gait cycle. The only exception is the spike at 15[kNm] of the healthy ankle, which corresponds to the impulse given during the push-off phase. Once again we realise that the torque values obtained in the simulation are too high for the reality.

5.3.3 Robustness test

The same robustness tests were applied to the flat ground prosthesis controller to assess it's ability to withstand perturbations.

Momentary force

The maximum momentary force the controller can withstand are available in Tab.5.1. The position the biped have at the beginning of each push can be visualised on Fig.5.4.

Continuous force

The continuous push tests, for the flat ground passive prosthesis adapted controller, gave the following results. A maximum continuous forward force of 75[N] and a backward force of -5[N] could be withstanded by the amputated biped before leading to a fall.

Slope variations

The slope variations test gave the following results, a positive maximum variation of $+1°$ and a negative variation of -5[°] could be withstanded before falling.

Discussion

By comparing the results of this section with the results of Section 3.4. We can assess that the controller designed for flat ground prosthesis adapted walking loses a little bit of resistance to forward pushes but this is compensated by an augmentation of the resistance to backward pushes in comparison with the controller designed for healthy biped.

However, this is not confirmed by the continuous push tests. Effectively, those tests highlight the opposite tendency.

For the slope tests, the prosthesis adapted controller did better than the original one in both ascending and descending.

Overall we can say that this controller is a little more robust than the controller designed for the healthy biped. We hypothesize that this may be due to the higher elevation of the feet during the swing phase leading to less unexpected contact with the floor during the slope variations test.

5.4 Results on slope ground

5.4.1 Kinematic results

A comparison of hip, knee and ankle angles between the simulations of the controller designed for healthy biped and the controller designed for passive prosthesis is shown on Fig.5.5 for the down slope controller and on Fig.5.6 for the up slope controller.

Discussion

As can be seen on the graphs the same kind of results than the one obtained for flat ground prosthesis adapted walking. Effectively, both the down slope and up slope controller have slightly larger thigh angles during the swing phase when compared to the controller without a prosthesis.

However the knee angle is almost the same for down slope whereas it is $\approx 40°$ higher for the up slope controller. We think that this is due to the fact that the up slope controller has to put the prosthesis at a particular angle compared to the ground as we can see on Fig.5.7. This allow to maximize the energy output of the prosthesis to have enough momentum to continue his up slope walk.

5.4.2 Robustness test

The same robustness tests were applied to the flat ground prosthesis controller. Those results will then be compared to the controllers designed for slopes with a healthy biped to assess the ability of the controllers designed in this chapter to withstand perturbation.

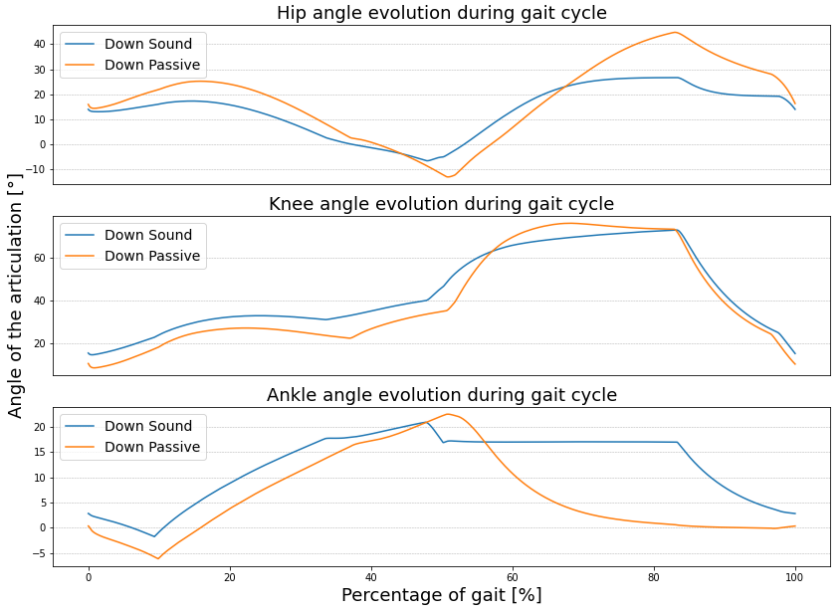

Figure 5.5: Comparison of the evolution of the angle of the hip, knee and ankle during a gait cycle on inclined down slope between the results of the simulation of the sound biped and the amputated biped

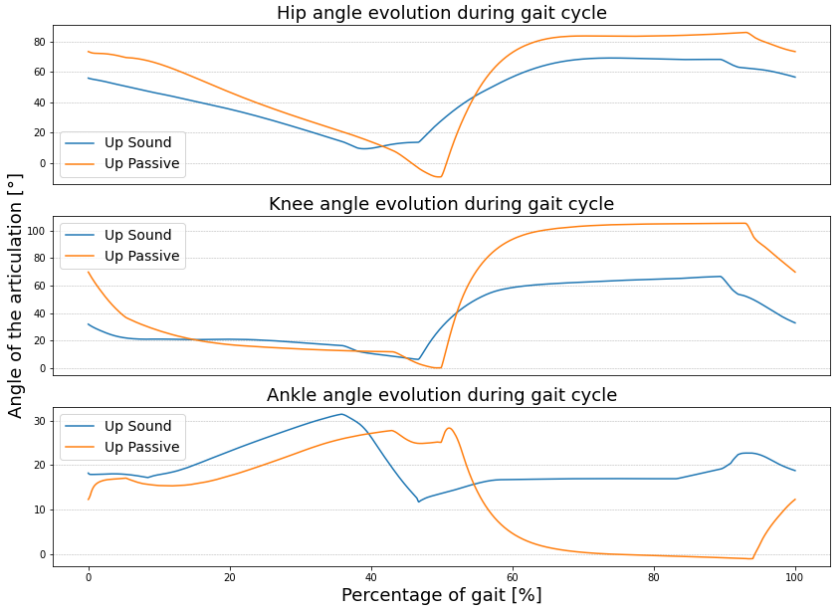

Figure 5.6: Comparison of the evolution of the angle of the hip, knee and ankle during a gait cycle on inclined up slope between the results of the simulation of a sound biped and an amputated biped

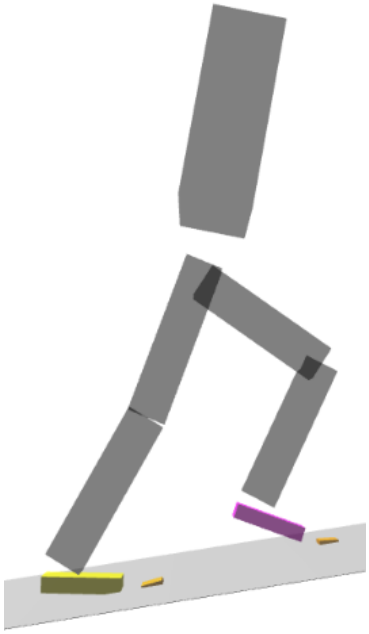

Figure 5.7: Diagram illustrating the angle of attack of the prosthesis during ascent with a passive prosthesis. Yellow = sound ankle; pink = passive prosthesis

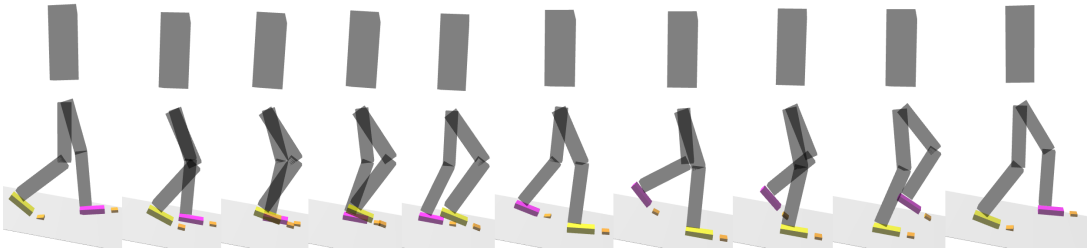

Figure 5.8: Visualisation of the posture of the biped when momentary force are applied from left to right 0% to 90%.

Momentary force

The maximum forces the controller can withstand are available in Tab.5.2. The positions of the biped when the force are applied can be visualised on Fig.5.9 & Fig.5.8.

Continuous force

For the continuous push tests, the down slope controller can withstand a maximum forward force of 30[N] and a maximum backward force of -5 [N]. For the up slope controller, the forward force is 75[N] and the backward force is -5[N].

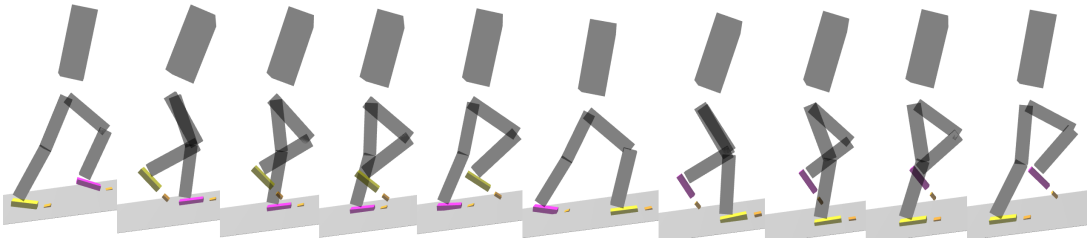

Figure 5.9: Visualisation of the posture of the biped when momentary force are applied from left to right 0% to 90%

	Time of application [% gait cycle]	0	10	20	30	40	50	60	70	80	90
Up slope	Forward max force [N]	250	250	200	150	100	1 50	750	675	375	250
Up slope	Backward max force [N]	-75	-125	-225	-400	-100	-100	-225	-400	-75	-50
Down slope	Forward max force [N]	250	250	200	150	100	150	750	675	375	250
Down slope	Backward max force [N]	-75	-125	-225	-4000	-100	-100	-225	-400	-75	-50

Table 5.2: Maximum force withstanded by the controller before falling.

Slope variations

The down slope controller is able to walk on slope from -7.25 to 12 [°] allowing a variation of +1.25 and -3.5 ° from the slope he was initially designed for. The up slope controller can withstand a variation of +4.75 or -1 [°].

Discussion

By comparing the results of this section with the results of Section 4.3.2, we can say that the controller designed for down slope passive prosthesis walking is slightly less robust to pushes than the one designed for a healthy biped. Effectively, it loses a good amount ($\approx -30\%$) of it's resistance to forward pushes and only gains a little bit of resistance to backward pushes($\approx +15\%$). However this loss is compensated by a slight increase in resistance to slope variations.

On the other hand, the controller designed for up slope passive prosthesis walking follows an opposite trend. Effectively he is more resistant to pushes in the forward direction($\approx +50\%$) and less resistant to pushes in the backward direction ($\approx -40\%$). Considering the continuous push, it is able to withstand three times more force in the forward direction and three times less force in the backward direction confirming the trend of the momentary forces.

For the slope variations test, it was not able to reproduce the astonishing results of -18° variations of the up slope controller for healthy biped as it can only withstand a negative variation of 1°. However, this controller has nothing to be jealous of as he set a new record of +4.75° of positive variation.

5.5 Conclusion

In conclusion, the controllers designed for walking with a passive prosthesis deviate more from the experimental data than the previous results. This was expected given the strategy implemented to prevent the toes of the ankle from touching the ground, which lead to more significant flexion of the thighs and knees.

From a stability standpoint, the controllers did not particularly gain or lose overall stability. However, their abilities to withstand certain disturbances changed depending on the controllers, and it might be interesting to leverage these results for future work as they may reveal valuable information.

Chapter 6

ELSA implementation

6.1 Introduction to ELSA

ELSA is a bionic prosthesis developed to provide trans-tibial (TT) amputees with a bio-inspired, user-friendly, lightweight, and energy-efficient solution at an affordable cost. The initial version of the ELSA prosthesis was designed at UCLouvain in 2017, incorporating a Spring-Motorized system that integrates a lockable parallel spring (LPS) and a series elastic actuator (SEA) leading to the V1 of ELSA prosthesis as shown on Fig.6.1.

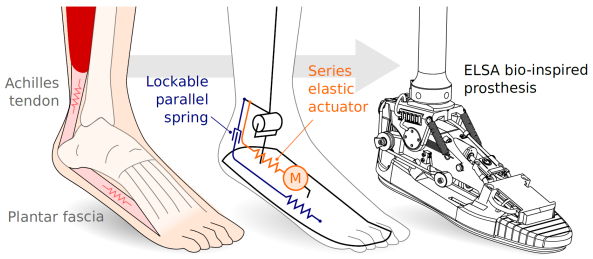

Figure 6.1: ELSA V1 bioinspired design [30]

At the core of the ELSA prosthesis are its internal mechanisms, each meticulously engineered to replicate natural ankle dynamics. The lockable parallel spring (LPS) is a passive mechanism that employs a nylon rope to store and release mechanical energy during gait. This mechanism, inspired by the configuration of the plantar fascia and Achilles tendon of the sound ankle, autonomously locks at the maximum plantarflexion angle (MPA) after heel strike. Complementing the LPS, a series elastic actuator (SEA) contributes the necessary net positive mechanical energy crucial for attaining a more natural gait.

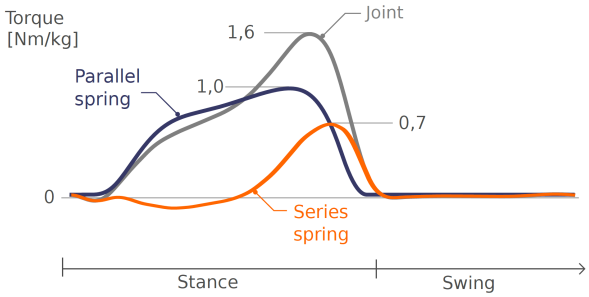

Figure 6.2: Normalized torque profile of the ankle during normal speed walking (grey), split between the contributions from a passive elastic element (blue) and a series elastic element with a 75kg subject

One of the ELSA prosthesis's strength is its power efficiency, particularly during the stance phase of the gait cycle. By combining the passive elasticity of the LPS with the active output of the SEA as is shwon in Fig.6.2, the prosthesis significantly reduces power consumption, enhancing user comfort and reducing the cognitive effort required for natural walking.

6.2 ELSA implementation

In order to test ELSA in the simulation, ELSA's digital twin was implemented in the simulation. The development of the digital twin was made prior to this work by the authors of the ELSA prosthesis.

Fig.6.4a shows the changes made to the MBsysPad environment to change the left leg of the biped by ELSA's digital twin. The length of ELSA's digital twin's tibia has been adjusted to match the length of the right leg of the biped to avoid any issues related to different leg lengths. The corresponding 3D model used for visualisation is illustrated in Fig.6.4b.

The internal mechanism of ELSA V2 are depicted on Fig.6.3. On this figure, we can see the compression spring linked to the nut carrier by the transmission rope. These parts of the prosthesis are equivalent to the LPS. In order to implement a simplified version of ELSA V2 in the simulation, we used a spring-damper system designed to replicate ELSA's regenerative mode mechanics. This mode of ELSA, where the SEA is not used, aims to avoid battery usage and thus saves energy.

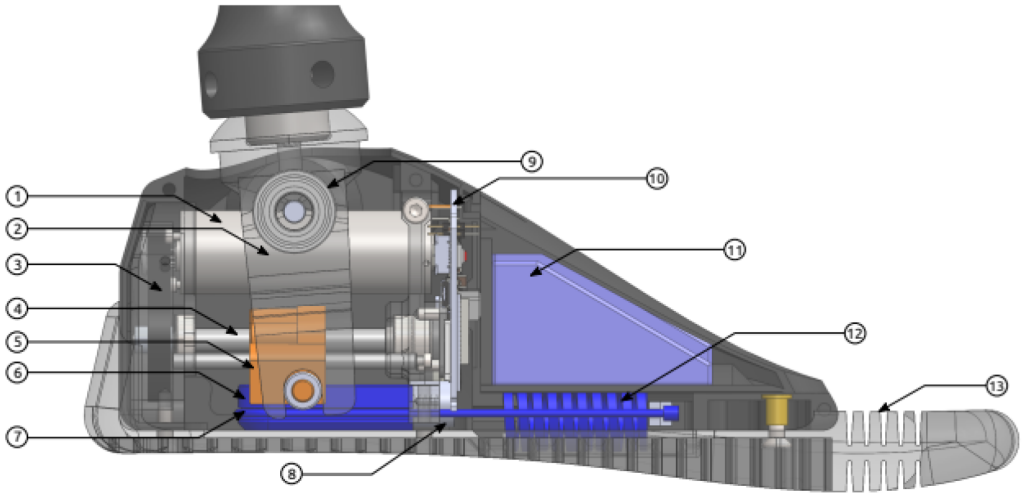

Figure 6.3: Section view of the internal mechanism of ELSA V2

1. motor
2. main lever
3. belt-pulley transmission
4. ball screw
5. nut carrier
6. locking mechanism
7. transmission rope
8. locker actuation coil
9. main ankle joint
10. control board
11. internal battery pack
12. compression spring
13. flexible toes insole

6.3 IMU implementation

There's an Inertial Measurement Unit (IMU) in the ELSA prosthesis. The IMU is connected to ELSA's controller to provide it with real-time linear acceleration and rotational velocity of the prosthesis. However, it digital twin does not have one. For further research on the prosthesis, it is important that both the physical version and the digital twin have the IMU. This section explains the changes made to the program to implement the IMU inside the emulator of the prosthesis.

An IMU is a device that measures and reports the specific force, angular rate and the orientation of the body on witch it is fixed by using a combination of accelerometers and gyroscopes. The goal of this thesis is to modify the code of the prosthesis emulator inside Robotran. The modified code has to get access and give access to the linear acceleration and the angular speed of the prosthesis to mimic the IMU inside the physical prosthesis.

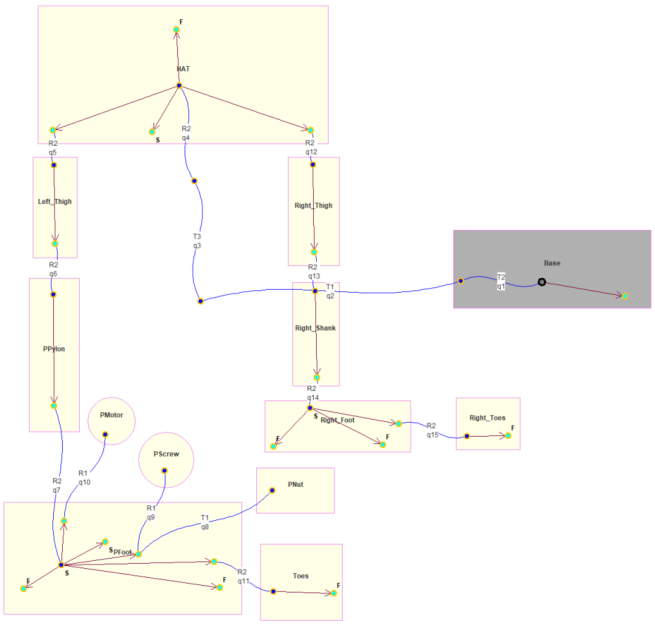

(a) ELSA biped model via Robotran MBsysPad

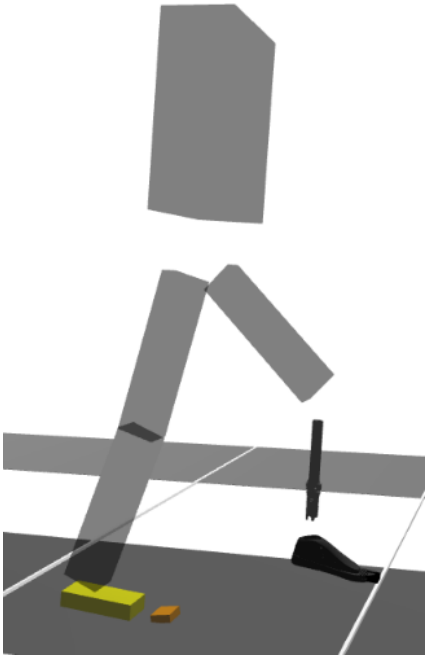

(b) 3D representation of the 7-links biped with ELSA replacing it left leg.

Figure 6.4: 7-link ELSA adapted biped presentation.

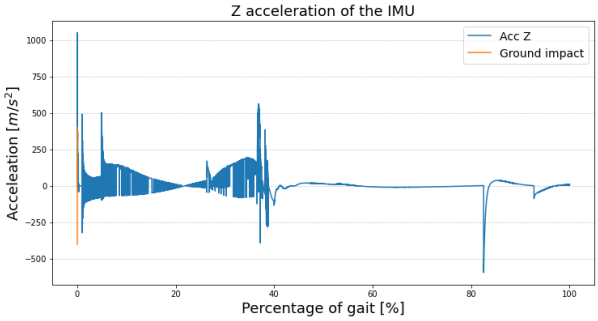

Figure 6.5: Graph of the vertical acceleration sent back by the IMU functions during a full gait cycle.

To implement the IMU a new structure "IMU.c" consisting of two functions was created. And as Fig.6.6 show, the functions of this structure are called inside the prosth emulator loop function which is used as its name tells to emulate the prosthesis inside Robotran. The first function is designed to compute the angular speed of the IMU while the second one is designed to compute the linear acceleration. To compute the linear acceleration and the angular speed of the IMU, it is necessary to multiply them by their rotation matrices. This is done with the help of the mbs_data structure passed as an argument of the functions. The mbs_data structure is as part of the Robotran environment. This structure contains the matrices of rotation, angular speed and linear acceleration of any point w.r.t., the original base frame of Robotran (see Fig.3.1).

As we can see on the diagram, the arrays containing the linear accelerations and the angular speeds are arguments of the function and the functions directly modifies the values of these vectors. To do so, two variables where created inside "prosth_emulator.c", "prosth.IMU_OM[4]" and "prosth.IMU_A[4]".

The other goal of the IMU implementation was the ability of "prosth_emulator.c" to be able to give back the two vectors computed by the IMU and this is done by the void functions "prosth_emulator_get_IMU_OM" and "prosth_emulator_get_IMU_A" which are designed the same way as the '"IMU_emulator_get_OM/A" functions.

6.3.1 IMU's Results

To get the results of the IMU in a similar way, the prosthetic controller will later use it. The functions implemented in the prosth_emulator.c are called in the simbicon_controller_loop function to test its capability to pass the vector values to another file. Fig.6.5 shows the vertical acceleration sent back by the IMU functions during a full-gait cycle.

Discussion

As can be seen on the graph, the most significant acceleration occurs precisely at the moment the foot impacts the ground which leads us to believe that the vertical accelerom-

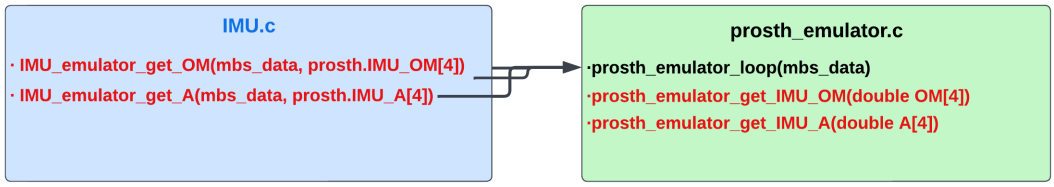

Figure 6.6: Diagram showing a simplified version of the IMU's implementation inside the program.

eter is functional. However, the angular velocities provided by the IMU are consistently zero. After investigation, we realized that the angular velocity vector returned by the 'mbs_data' structure is consistently zero as well. Therefore, we believe that the issue originates from there. Considering that both functions have exactly the same implementation, there is no reason for one to work while the other does not.

6.4 Results on flat ground

No results from the robustness tests are available in this chapter, as the obtained results were almost identical to the outcome of the previous chapter. Therefore, we judged them uninteresting to present.

A comparison of hip, knee and ankle angles between the simulations of the controllers designed for passive prosthesis and the controller designed for ELSA prosthesis is shown in Fig.6.7.

Discussion

On the graph, we can see that the angles of the thigh and the knee are almost identical, which is quite expected since the controller underwent no changes between the two simulations. However, it can be observed that ELSA's maximum ankle dorsiflexion angle is larger than the one of the passive prosthesis (reaching a minimum of -10ř at the moment of impact), which is a positive outcome as it'll allow ELSA to generate more power with the LPS.

6.5 Results on slope ground

A comparison of hip, knee and ankle angles between the simulations of the controllers designed for passive prosthesis slope walking and the controller designed for ELSA prosthesis slope walking is shown in Fig.6.8 & Fig.6.9.

Discussion

The results for the thighs and knees are the same in both case. However, we can observe something new thanks to these graphs. Indeed, we can see that the ELSA angle never goes

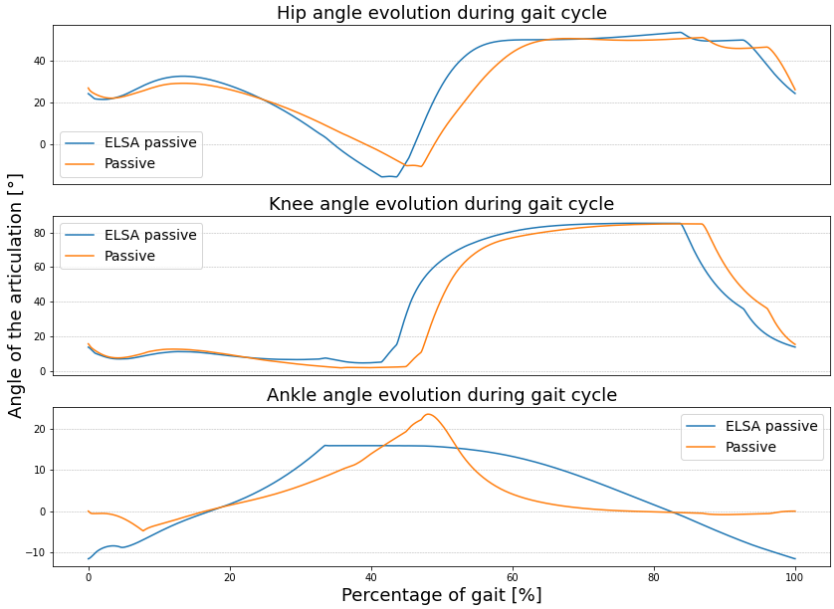

Figure 6.7: Comparison of the evolution of the angle of the hip, knee and ankle during a gait cycle on flat ground between the results of the simulation of the passive prosthesis biped and the ELSA prosthesis biped

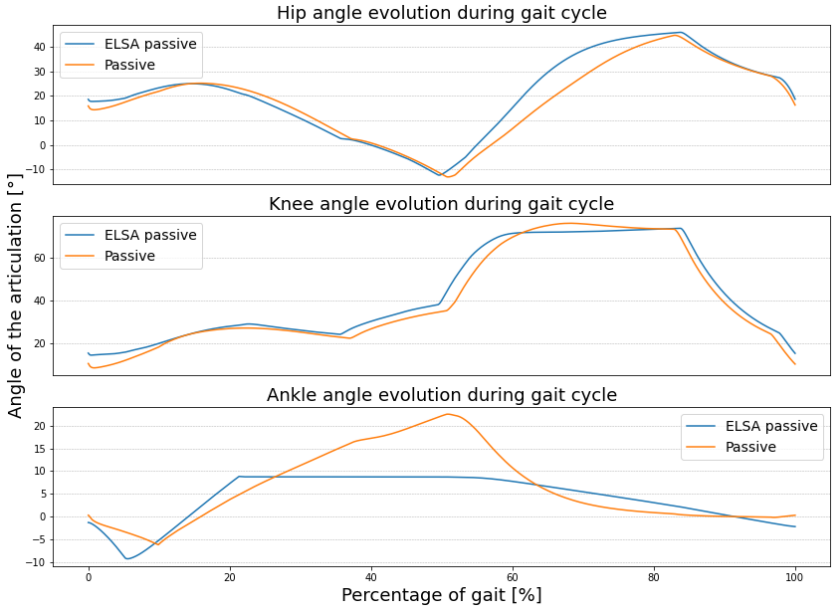

Figure 6.8: Comparison of the evolution of the angle of the hip, knee and ankle during a gait cycle on inclined down slope between the results of the simulation of the passive prosthesis biped and the ELSA prosthesis biped

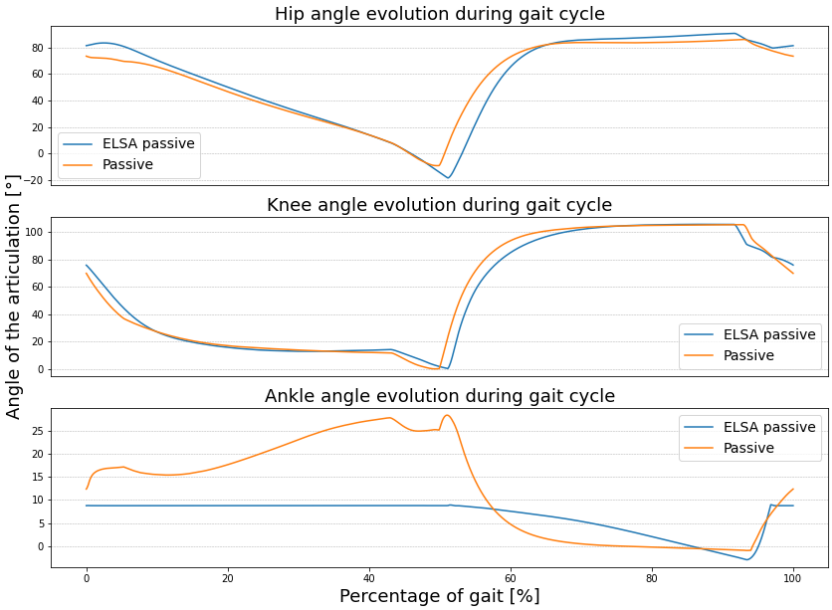

Figure 6.9: Comparison of the evolution of the angle of the hip, knee and ankle during a gait cycle on inclined up slope between the results of the simulation of the passive prosthesis biped and the ELSA prosthesis biped

above 10° for simulations on sloped ground and we believe that this is linked to ELSA's internal mechanism, which prevents excessive plantar flexion. ELSA was implemented as a simple linear spring placed at the level of the nut carrier but this implies that the entire internal mechanics of ELSA are fully operational in this simulation, as shown by these results.

6.6 Conclusion

In conclusion the controllers designed to walk with the passive prosthesis were also able to walk with ELSA's digital twin. And the results obtained were very similar. The comparison of the results between these simulation allowed us to highlight a difference that lies between ELSA's prosthesis and a normal passive prosthesis. Finally, we think that the resulting environment developed through this thesis is able to simulate biped walking in a digitized environment. However many upgrades can still be done on the basis of this work to simulate more complicated cases.

Conclusion

In this thesis, we introduced an environment capable of simulating human gait. Within this environment, we designed a controller capable of manipulating the joints of a 7-link bipedal walker. By utilizing scientific data, we subsequently validated this controller. Ultimately, we integrated the digital twin of the ELSA prosthesis into this same environment to conduct tests on it.

In the first chapter, we began by providing the current scientific context upon which this work is based. In this chapter, we examined the impacts that digital twins already have on our environment today and described their effects. Subsequently, we presented various methods for simulating the human gait.

In the second chapter, we introduced the SIMBICON model. We started with a description of its balance control strategy, which enabled us to introduce the concept of FSM (Finite State Machine), along with the key operational principles of this model. Then, through a comparison with scientific data, we highlighted the main weaknesses of SIMBICON.

In the third chapter, we introduced an adapted model of SIMBICON, enhancing the model's kinematics to better align with scientific data. In this chapter, we began with a brief explanation of the implementation of the virtual environment and the "7-links" biped. Next, we presented the ground contact model used in this work. Then, we introduced the "6 state FSM" developed during this thesis and concluded with a presentation of the results. These results focused on three aspects: kinematics, dynamics and the robustness of the developed controller. By comparing these outcomes to scientific data, we were able to identify the weaknesses of our controller.

The fourth chapter focuses on improving the controller's ability to walk on inclined terrain. Here, we describe the modifications made to the decision tree to achieve this new version. Subsequently, we present the results and compare them through a discussion with experimental data.

In the fifth chapter we discussed the controller's adaptation to walking with a passive prosthesis. In this chapter, we carried out the same tests as in the previous chapters to compare the results with those of the earlier chapters. This highlighted the changes brought to the controller to enable him to walk with a prosthesis.

In the final chapter, we briefly introduced the functioning of the ELSA prosthesis. Furthermore we proceeded with an explanation of the implementation of ELSA's digital twin in the virtual environment, along with the integration of the IMU within this digital twin. Subsequently, we analyzed the results obtained from the IMU to validate its functionality. We concluded with a comparison of the outcomes between the ELSA prosthesis and the passive prosthesis.

This work enabled us to develop a simulator for human walking within an environment. This tool will already allow the ELSA prosthesis development team to conduct simulations for testing specific functionalities. However, we believe there is room for further improvements to allow a greater variety of simulations.

Outlook for the future

As stated in the conclusion, this research has laid the foundations for an environment capable of simulatinf the human gait in a digitized environment. Nevertheless, we believe that there is still work to be done before achieving a tool that can fully assist in prosthesis design. Thus, we will discuss a few avenues for improvement that came to mind during the course of this work.

To begin with, we believe that implementing a controller that adjusts its target angles based on the slope angle could be very interesting. As observed in this thesis, with the exception of one set of angles that enabled the controller to perform well both uphill and downhill, all the other controllers are highly sensitive to variations in slope. Therefore, implementing such a controller would be intriguing as it would allow testing ELSA's digital twin in numerous scenarios that are currently inaccessible.

Furthermore, as you have seen, there are certain issues with the contact model. Now that the controller is implemented, it might be worthwhile to change this contact model in order to obtain results that are more coherent with reality. Nevertheless, this is not crucial since the force spikes are very brief and don't significantly impact the simulation.

Lastly, we have considered the use of artificial intelligence to find the optimal parameters that would bring the greatest stability while staying close to the kinematic of the human gait. In fact, a significant amount of time was devoted to the research of parameters enabling walking on flat ground first, then on sloped surfaces, and so forth. Behind each of these modes lies hours of work aimed at getting as close as possible to the kinematics of human walking. All of this effort likely still didn't yield the best parameters in the end. This is why we believe that with artificial intelligence, it could be possible to optimize parameters such as :the target angles, the time spent in a given state, or even create controllers with more states to allow for more freedom in angle selection. This could potentially lead to a controller that outperforms the one developed in this study.

Bibliography

[1] Xiling Lin, Yufeng Xu, Xiaowen Pan, Jingya Xu, Yue Ding, Xue Sun, Xiaoxiao Song, Yuezhong Ren, and Peng-Fei Shan. Global, regional, and national burden and trend of diabetes in 195 countries and territories: an analysis from 1990 to 2025. 10(1):14790.

[2] Yuqi Zhang, Peter A. Lazzarini, Steven M. McPhail, Jaap J. van Netten, David G. Armstrong, and Rosana E. Pacella. Global disability burdens of diabetes-related lower-extremity complications in 1990 and 2016. 43(5):964–974.

[3] Oana Chiriac and Doina Bucur. From conventional prosthetic feet to bionic feet. a review. pages 130–138.

[4] Sebastian Haag and Reiner Anderl. Digital twin proof of concept. 15.

[5] Bin He and Kai-Jian Bai. Digital twin-based sustainable intelligent manufacturing: a review. 9.

[6] Sin Yong Teng, Michal Tou, Wei Dong Leong, Bing Shen How, Hon Loong Lam, and Vítzslav Máa. Recent advances on industrial data-driven energy savings: Digital twins and infrastructures. 135:110208.

[7] Georgios Mylonas, Athanasios Kalogeras, Georgios Kalogeras, Christos Anagnostopoulos, Christos Alexakos, and Luis Muñoz. Digital twins from smart manufacturing to smart cities: A survey. 9:143222–143249. Conference Name: IEEE Access.

[8] Maged N. Kamel Boulos and Peng Zhang. Digital twins: From personalised medicine to precision public health. 11(8):745.

[9] Hongchao Shu, Ruixing Liang, Zhaoshuo Li, Anna Goodridge, Xiangyu Zhang, Hao Ding, Nimesh Nagururu, Manish Sahu, Francis X. Creighton, Russell H. Taylor, Adnan Munawar, and Mathias Unberath. Twin-s: a digital twin for skull base surgery. 18(6):1077–1084.

[10] Michael G. Bateman, William K. Durfee, Tinen L. Iles, Cindy M. Martin, Kenneth Liao, Arthur G. Erdman, and Paul A. Iaizzo. Cardiac patientspecific threedimensional models as surgical planning tools. 167(2):259–263.

[11] Maulshree Singh, Evert Fuenmayor, Eoin Hinchy, Yuansong Qiao, Niall Murray, and Declan Devine. Digital twin: Origin to future. 4:36.

[12] Michael Grieves and John Vickers. Digital twin: Mitigating unpredictable, undesirable emergent behavior in complex systems. pages 85–113.

[13] Werner Kritzinger, Matthias Karner, Georg Traar, Jan Henjes, and Wilfried Sihn. Digital twin in manufacturing: A categorical literature review and classification. 51(11):1016–1022.

[14] Azad Madni, Carla Madni, and Don Lucero. Leveraging digital twin technology in model-based systems engineering. 7:7.

[15] Matthew Abdel, Philipp von Roth, Matthew Jennings, Arlen Hanssen, and Mark Pagnano. What safe zone? the vast majority of dislocated THAs are within the lewinnek safe zone for acetabular component position. 474.

[16] Matthew Handford and Manoj Srinivasan. Robotic lower limb prosthesis design through simultaneous computer optimizations of human and prosthesis costs. 6:19983.

[17] Mahdokht Ezati, Borna Ghannadi, and John McPhee. A review of simulation methods for human movement dynamics with emphasis on gait. 47(3):265–292.

[18] Yujiang Xiang, Jasbir S. Arora, and Karim Abdel-Malek. Physics-based modeling and simulation of human walking: a review of optimization-based and other approaches. 42(1):1–23.

[19] Sajid Iqbal, Xizhe Zang, Yanhe Zhu, and Jie Zhao. Bifurcations and chaos in passive dynamic walking: A review. 62(6):889–909.

[20] Steve Collins, Andy Ruina, Russ Tedrake, and Martijn Wisse. Efficient bipedal robots based on passive-dynamic walkers. 307:1082–5.

[21] Nicolas Van der Noot and Allan Barrea. *Zero-Moment Point on a bipedal robot under bio-inspired walking control*. Pages: 90.

[22] Michael Andersen, Michael Damsgaard, and John Rasmussen. A study of the effects of two different kinematical analysis methods on the calculated muscle activities in an inverse dynamics-based musculoskeletal model of gait.

[23] KangKang Yin, Kevin Loken, and Michiel van de Panne. SIMBICON: simple biped locomotion control. 26(3):105–es.

[24] Gabriele Bovi, Marco Rabuffetti, Paolo Mazzoleni, and Maurizio Ferrarin. A multiple-task gait analysis approach: Kinematic, kinetic and EMG reference data for healthy young and adult subjects. 33(1):6–13.

[25] Simbicon project webpage.

[26] David A. Winter. *Biomechanics and motor control of human movement*. Wiley, 4th ed edition. OCLC: ocn318408191.

[27] Sören Andersson, Anders Söderberg, and Stefan Björklund. Friction models for sliding dry, boundary and mixed lubricated contacts. 40(4):580–587.

[28] Steven J Levitz. Pressure analysis of the foot in gait.

[29] Andrea N. Lay, Chris J. Hass, and Robert J. Gregor. The effects of sloped surfaces on locomotion: A kinematic and kinetic analysis. 39(9):1621–1628.

[30] François Heremans, Sethu Vijayakumar, Mohamed Bouri, Bruno Dehez, and Renaud Ronsse. *Bio-inspired design and validation of the Efficient Lockable Spring Ankle (ELSA) prosthesis*, volume 2019. Journal Abbreviation: IEEE ... International Conference on Rehabilitation Robotics : [proceedings] Pages: 416 Publication Title: IEEE ... International Conference on Rehabilitation Robotics : [proceedings].

Appendix A

A.1 Body segment lengths

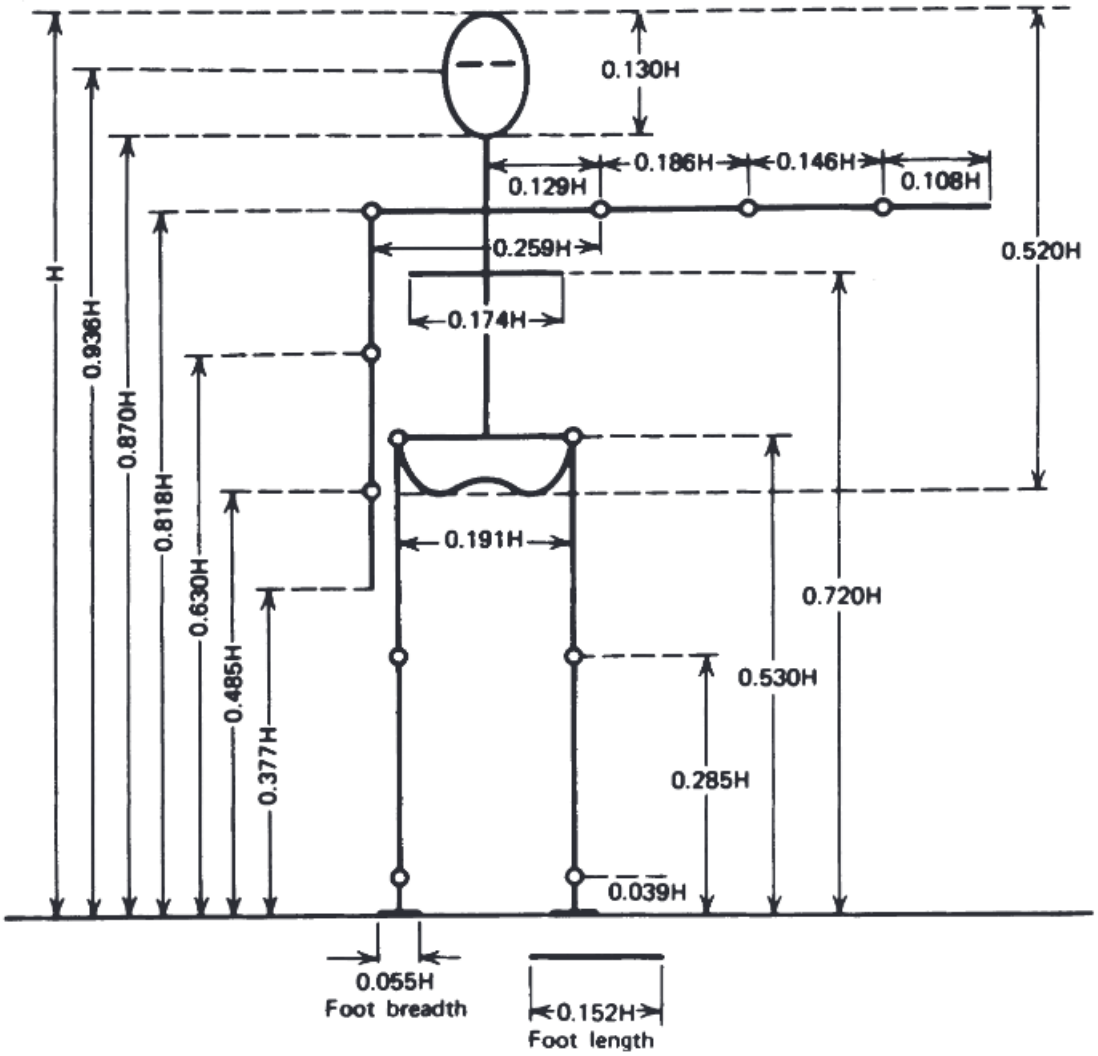

A.2 Anthropometric Data

TABLE 4.1 Anthropometric Data

Segment	Definition	Segment Weight/Total Body Weight	Center of Mass/ Segment Length		Radius of Gyration/ Segment Length			Density
			Proximal	Distal	C of G	Proximal	Distal	
Hand	Wrist axis/knuckle II middle finger	0.006 M	0.506	0.494 P	0.297	0.587	0.577 M	1.16
Forearm	Elbow axis/ulnar styloid	0.016 M	0.430	0.570 P	0.303	0.526	0.647 M	1.13
Upper arm	Glenohumeral axis/elbow axis	0.028 M	0.436	0.564 P	0.322	0.542	0.645 M	1.07
Forearm and hand	Elbow axis/ulnar styloid	0.022 M	0.682	0.318 P	0.468	0.827	0.565 P	1.14
Total arm	Glenohumeral joint/ulnar styloid	0.050 M	0.530	0.470 P	0.368	0.645	0.596 P	1.11
Foot	Lateral malleolus/head metatarsal II	0.0145 M	0.50	0.50 P	0.475	0.690	0.690 P	1.10
Leg	Femoral condyles/medial malleolus	0.0465 M	0.433	0.567 P	0.302	0.528	0.643 M	1.09
Thigh	Greater trochanter/femoral condyles	0.100 M	0.433	0.567 P	0.323	0.540	0.653 M	1.05
Foot and leg	Femoral condyles/medial malleolus	0.061 M	0.606	0.394 P	0.416	0.735	0.572 P	1.09
Total leg	Greater trochanter/medial malleolus	0.161 M	0.447	0.553 P	0.326	0.560	0.650 P	1.06
Head and neck	C7–T1 and 1st rib/ear canal	0.081 M	1.000	— PC	0.495	0.116	— PC	1.11
Shoulder mass	Sternoclavicular joint/glenohumeral axis	—	0.712	0.288	—	—	—	1.04
Thorax	C7–T1/T12–L1 and diaphragm*	0.216 PC	0.82	0.18	—	—	—	0.92
Abdomen	T12–L1/L4–L5*	0.139 LC	0.44	0.56	—	—	—	—
Pelvis	L4–L5/greater trochanter*	0.142 LC	0.105	0.895	—	—	—	—
Thorax and abdomen	C7–T1/L4–L5*	0.355 LC	0.63	0.37	—	—	—	—
Abdomen and pelvis	T12–L1/greater trochanter*	0.281 PC	0.27	0.73	—	—	—	1.01
Trunk	Greater trochanter/glenohumeral joint*	0.497 M	0.50	0.50	—	—	—	1.03
Trunk head neck	Greater trochanter/glenohumeral joint*	0.578 MC	0.66	0.34 P	0.503	0.830	0.607 M	—
Head, arms, and trunk (HAT)	Greater trochanter/glenohumeral joint*	0.678 MC	0.626	0.374 PC	0.496	0.798	0.621 PC	—
HAT	Greater trochanter/mid rib	0.678	1.142	—	0.903	1.456	—	—

*NOTE: These segments are presented relative to the length between the greater trochanter and the glenohumeral joint.

Source Codes: M, Dempster via Miller and Nelson; *Biomechanics of Sport*, Lea and Febiger, Philadelphia, 1973. P, Dempster via Plagenhoef; *Patterns of Human Motion*, Prentice-Hall, Inc. Englewood Cliffs, NJ, 1971. L, Dempster via Plagenhoef from living subjects; *Patterns of Human Motion*, Prentice-Hall, Inc., Englewood Cliffs, NJ, 1971. C, Calculated.

A.3 Target angles table

			Slope [rad]	Torso	Hip Switch Angle	Posbalance	Sw Hip 0	Sw Hip 1	Sw Hip 2	St Knee 0	St Knee 1	St Knee 2	Sw Knee 0	Sw Knee 1	Sw Knee 2	St Ankle 0	St Ankle 1	St Ankle 2	Sw Ankle 0	Sw Ankle 1	Sw Ankle2
Natural gait	Normal ground		0	0,03	0,1	1,9	0,5	0,45	0,45	0,14	0,24	0,28	1,15	0,2	0,1	0,2	0	-0,5	0,3	0	0
	Down slope		-0,1483	0	0,05	1,9	0,3	0,15	0,9	0,4	0,7	0,4	1,3	0,2	0,1	0,2	0	-0,5	0,3	0	0
	Up slope		0,1483	0,14	0,25	1,9	1,1	0,7	0	0,38	0,1	0,1	1,15	0,2	0,1	0,2	0	-0,8	0,3	0,3	0
Prosthesis adapted gait	Normal ground	Jambe saine R	0	0,06	0,1	1,9	0,8	0,7	0,1	0,14	0,24	0,28	1,5	0,4	0,1	0,2	0	-0,5	0,3	0	0
		Jambe amputée L					0,8	0,7	0,1	0,14	0,24	0,28	1,5	0,4	0,1	0	0	0	0	0	0
	Down slope	Jambe saine R	-0,1483	0	0,05	1,9	0,6	0,15	0,9	0,4	0,7	0,4	1,3	0,4	0,1	0,2	0	-0,5	0,3	0	0
		Jambe amputée L					0,6	0,15	0,9	0,4	0,7	0,4	1,3	0,4	0,1	0	0	0	0	0	0
	Up slope	Jambe saine R	0,1483	0,15	0,15	1,9	1,6	1,05	0,65	0,38	0,1	0,1	1,85	0,8	0,1	0,2	0	-0,8	0,3	0	0
		Jambe amputée L					1,6	1,05	0,65	0,38	0,1	0,28	1,85	0,8	0,1	0	0	0	0	0	0

UNIVERSITÉ CATHOLIQUE DE LOUVAIN
École polytechnique de Louvain
Rue Archimède, 1 bte L6.11.01, 1348 Louvain-la-Neuve, Belgique | **www.uclouvain.be/epl**